Experimental investigation and thermodynamic assessment of the $BaCl_2$–$CeCl_3$ system

Alders, D. C.; Vlieland, J.; Thijs, M.; Konings, R. J.M.; Smith, A. L.

DOI
10.1016/j.molliq.2024.123997

Publication date
2024

Document Version
Final published version

Published in
Journal of Molecular Liquids

Journal of Molecular Liquids 396 (2024) 123997

Contents lists available at ScienceDirect

Journal of Molecular Liquids

journal homepage: www.elsevier.com/locate/molliq

Experimental investigation and thermodynamic assessment of the $BaCl_2$–$CeCl_3$ system

D.C. Alders, J. Vlieland, M. Thijs, R.J.M. Konings, A.L. Smith *

Delft University of Technology, Faculty of Applied Sciences, Radiation Science & Technology Department, Mekelweg 15, 2629 JB Delft, the Netherlands

ARTICLE INFO

Keywords:
Molten salts
CALPHAD
Chloride salts
Cerium chloride
Barium chloride

ABSTRACT

The thermodynamic and thermo-physical properties of the molten salt system $BaCl_2$–$CeCl_3$ have been investigated using an experimental and modelling approach. This molten salt system includes a single intermediate compound $Ba_3Ce_2Cl_{12}$, whose structure has been investigated using X-ray and neutron diffraction. Furthermore, this system exhibits solubility of $CeCl_3$ in $BaCl_2$ at high temperatures up to a concentration of around 25% $CeCl_3$ at 1060 K. Additionally, our measurements show solubility of $BaCl_2$ in $CeCl_3$ up to about 5% $BaCl_2$ at 973 K. The investigation of these solid solutions has been performed using quenching experiments and subsequent post-characterisation by X-ray diffraction (XRD). Phase diagram equilibria have also been investigated using differential scanning calorimetry (DSC). Using the aforementioned information on phase transitions, intermediate compound formation, and mutual solid solubility, a thermodynamic assessment of the system has been performed using the CALPHAD method. The model for the Gibbs energy of the liquid solution is the quasi-chemical formalism in the quadruplet approximation, while the model for the Gibbs energy of the solid solutions is a two-sublattice polynomial model.

1. Introduction

The development of Molten Salt Reactor (MSR) technology requires a comprehensive understanding of the physical and chemical properties of the molten fuel salt, as well as predictive modelling capabilities of its behaviour during normal reactor operation and off-normal operating conditions. Over the last decade, a renewed interest in the MSR concept has emerged, with numerous studies reporting fluoride mixtures that are appealing because of their low vapor pressures and high thermochemical stability at elevated temperatures [1,2]. More recently, chloride salts have also garnered attention as potential candidates for molten salt fuels as they can provide higher actinide solubility and lower melting temperatures of the fuel salt mixtures [3], potentially increasing the safety margin during operation. During irradiation, numerous fission products are generated, making the fuel a multi-component system, and affecting its thermochemical and thermophysical properties. Thermochemical modelling can be used to predict the properties of multi-element systems by extrapolation of binary and ternary subsystems, but for this, a solid understanding of the basic thermochemistry of the constituting binaries and ternaries is first needed.

One of the limiting factors for the development of a chloride-based molten salt reactor is the absence of a large knowledge base as is the case for fluoride salts [4] on thermodynamic and thermophysical properties such as melting temperatures, heat capacity, density or viscosity. While there is some basic data available, such as the melting behaviour of the system NaCl–$PuCl_3$ [5], the effect of fission products on the thermochemical properties of the molten chloride fuel has not been investigated as abundantly. Fission products are present in a molten salt system as one of three classes: salt-solubles, metallic precipitates or volatile fission products. For the assessment of the thermochemical properties of a molten salt fuel, salt-soluble fission products such as barium, strontium and rare earth metals are of particular interest because of their relatively high fission yield. The work presented here aims to contribute to this goal by adding to the thermochemical knowledge on the molten salt fission product system $BaCl_2$–$CeCl_3$, with both experimental investigations and thermodynamic modelling assessment by the CALPHAD (CALculation of PHase Diagrams) method. The interest in this system stems from the fact that both Ba and Ce are fission products, but also because cerium is sometimes used as a simulant for plutonium [6]. Using $CeCl_3$ as a simulant for more complex systems than this binary, i.e. when extrapolating to higher order systems, al-

* Corresponding author.
E-mail address: a.l.smith@tudelft.nl (A.L. Smith).

https://doi.org/10.1016/j.molliq.2024.123997
Received 22 September 2023; Received in revised form 8 December 2023; Accepted 6 January 2024
Available online 15 January 2024

lows the investigation of these systems without having to use the more hazardous $PuCl_3$.

Experimental investigations using X-ray and neutron diffraction, quenching experiments, and Differential Scanning Calorimetry (DSC) have first been performed to solve discrepancies noticed in the literature. Using those data as input, a CALPHAD model has then been developed based on the quasi-chemical formalism in the quadruplet approximation for the liquid solution, and a two-sublattice polynomial model for the solid solutions. In this process, mixing enthalpies of the liquid solution have also been estimated, as these data have not been measured experimentally to this date, but constitute a key piece of information to develop physically accurate liquid models.

2. Experimental techniques

2.1. Sample preparation and $Ba_3Ce_2Cl_{12}$ synthesis

For the experiments carried out in this work, $BaCl_2$ (Alfa Aesar, ultra-dry, 99.999% trace metals basis) and $CeCl_3$ (Alfa Aesar, ultra-dry, 99.9% trace metals basis) were used as delivered by the supplier. Due to the sensitivity of the salts towards oxygen and water, all sample preparation was carried out in a glove box under dry argon atmosphere ($H_2O, O_2 < 5$ ppm).

Weighing was carried out using a Mettler-Toledo XPE105DR balance with a 0.01 mg uncertainty. $Ba_3Ce_2Cl_{12}$ was synthesised by mixing the end members $BaCl_2$ and $CeCl_3$ in a stoichiometric ratio of 3:2 in an agate mortar, followed by thermal treatment in a tubular furnace under argon flow for eight to twelve hours at a temperature of 900 K. The sample was heated inside a tightly closed stainless steel container, with an inner nickel liner to prevent the corrosive chlorides from interacting with the stainless steel.

No additional phases were detected by X-ray diffraction (XRD) or neutron diffraction (ND) analysis, and the sample purity is expected to be better than 99%. The melting points of the end-members have been measured by DSC, and the obtained values are (1237 ± 5) K for $BaCl_2$ and (1087 ± 5) K for $CeCl_3$. This is in good agreement with the values reported in the literature for these salts, with (1235 ± 1) K [7] and (1090 ± 2) K [8], respectively.

2.2. X-ray diffraction

XRD measurements were carried out using a PANalytical X'pert pro diffractometer with a Cu-anode (0.4 mm x 12 mm line focus, 45 kV, 40 mA). Scattered X-ray intensities were measured with a real time multi step detector (X'Celerator). The angle 2θ was set to range from 10-120^o. Measurements were typically performed for 7-8 hours, with a step size of 0.0036^o/s. Refinement of the measured structures was performed by applying the refinement technique from Rietveld, Loopstra and van Laar [9,10], using the FullProf software, Version January 2023 [11].

2.3. Neutron diffraction

Neutron diffraction data were obtained at room temperature at the PEARL beamline at the Hoger Onderwijs Reactor at the Delft University of Technology [12]. The sample was contained in a vanadium cylindrical container (50 mm high, 6 mm inner diameter), closed with a Viton O-ring in the dry argon atmosphere of the glovebox. The data were collected at a fixed wavelength of 1.667 Å for 11 h with an angle 2θ ranging from 10-160^o. The data analysis was performed using the structural refinement method by Rietveld, Loopstra and van Laar [9,10] using the FullProf software [11].

2.4. Differential scanning calorimetry

The invariant temperatures in the $BaCl_2$–$CeCl_3$ system were measured using a Setaram multi-detector high temperature calorimeter (MHTC-96 type) equipped with a 3D heat flux DSC module and S-type thermocouples, capable of measuring up to 1673 K. Sample preparation was done by mixing end-members $BaCl_2$ and $CeCl_3$ in the desired stoichiometric ratio. The samples were contained in a nickel liner, which in turn was contained in a tightly closed stainless steel crucible. Equilibration of the sample was done in the calorimeter itself during the first heating cycle by heating the mixtures to a temperature above the melting points of both end-members. Invariant equilibria were collected on the subsequent heating cycles.

The temperatures were monitored throughout the experiments by a series of interconnected S-type thermocouples. The temperature on the heating ramp (10 K · min^{-1}) was calibrated and corrected for the effect of the heating rate by measuring the melting points of standard high purity metals (In, Sn, Pb, Al, Ag, Au) at 2-4-6-8-10-12 K · min^{-1}. The calibration procedure was performed as recommended by Höne et al. [13] and Gatta et al. [14]. The transition temperatures in the $BaCl_2$–$CeCl_3$ phase diagram were derived on the heating ramp as the onset temperature using tangential analysis of the recorded heat flow. The liquidus temperature of mixtures was derived from the peak extremum of the last thermal event. The uncertainty on the measured temperatures is estimated to be ± 5 K for pure compounds and ±10 K for mixtures.

2.5. Investigation of solid solutions

The existence and stability range of solid solutions in the $BaCl_2$–$CeCl_3$ system were investigated in this work using quenching experiments. The quenching samples consisted of stoichiometric mixtures of the end-members, thoroughly mixed using a pestle and mortar before insertion inside a nickel liner in a tightly closed stainless steel crucible. During the experiments, the samples were heated to selected temperatures ranging from 1023 to 1273 K and equilibrated at this temperature for at least one hour, after which they were dropped into a water bath to freeze the phases stable at high temperature.

The furnace used for quenching is an MTI split vertical quenching tube furnace (OTF-1500X-80-VTQ), which contains an electromagnet that holds the sample in the heated part of the furnace. When the sample is at the desired temperature and has been allowed to reach equilibrium, the electromagnet is shut off and the sample drops into the water bath.

2.6. Solution calorimetry

The dissolution enthalpy of the intermediate $Ba_3Ce_2Cl_{12}$ was measured using a TA Instruments Precision Solution Calorimeter (semi-adiabatic or isoperibolic calorimeter) and a TAM IV thermostat. The experimental setup consists of a 25 mL Pyrex glass reaction vessel and a motorized gold stirrer. The temperature change during the dissolution of $Ba_3Ce_2Cl_{12}$ was monitored with a thermistor, while a heater was used for calibration during the measurement and equilibration of the initial baseline in the optimal operating range of the calorimeter (25 ± 0.3 K) before starting the experiment. The sample container was a 1 mL glass ampoule sealed airtight using beeswax. Sample preparation was performed inside the dry argon atmosphere of the glovebox, with the airtight sealing being performed in air. The salt was dissolved in 25 mL H_2O by breaking the bottom of the glass ampoule on the sapphire breaking tip mounted on the bottom of the reaction vessel. The heat of breaking of the glass is exothermic with an energy below 10 mJ, and can thus be neglected. The temperature during measurements was maintained in an oil bath with an accuracy of 10^{-4} K. Electrical calibrations were performed before and after each enthalpy measurement, so as to determine the energy equivalent of the system. These calibrations consisted of introducing a heat pulse of approximately the same magnitude as the (expected) enthalpy of dissolution (i.e. 15 J) and gauging the temperature effect this had on the reaction vessel.

The enthalpy of dissolution of KCl (Sigma Aldrich, 99.7%) in 1000H_2O (distilled water) (molality $m = 0.05551$ mol · kg^{-1}) was first

Table 1
Thermodynamic functions used in the CALPHAD model in this work. The heat capacity is expressed as the following polynomial: $C_{p,m}(T) = a + bT + cT^{-2} + dT^2$. Optimized values are marked in bold.

Compound	$\Delta_f H^o_m(298)$ ($J \cdot mol^{-1}$)	$S^o_m(298)$ ($J \cdot K^{-1} \cdot mol^{-1}$)	$C_{p,m}(T)$ ($J \cdot K^{-1} \cdot mol^{-1}$) = a + bT + cT^{-2} + dT^2				Temperature range (K)	Source
			a	b	c	d		
α-$BaCl_2$(s)	−855,200	123.7	69.371	0.01912548	5882.698	$2.499235 \cdot 10^{-9}$	[298-1198]	[20]
β-$BaCl_2$(s)	−837,800	138.22	131				[1198-1234]	[20]
$BaCl_2$(l)	−821,950	151.07	109				[1234-2500]	[20]
$CeCl_3$(s)	−1,059,700	151	90.9772	0.0358123	−271,530		[298-1095]	[8]
$CeCl_3$(l)	−1,006,100	200.17	161.05				[1095-3000]	[8]
$Ba_3Ce_2Cl_{12}$	**-4,711,000**	**689.5**	390.07	0.129	−525,411.69	$7.4977 \cdot 10^{-9}$	[298-2500]	This work

measured to check the instrument accuracy, which yielded $\Delta_{diss}H^o_m$ ($1000H_2O$, 298.15 K) = 17.510 ± 0.024 kJ · mol^{-1}. This corresponds to a dissolution enthalpy in $500H_2O$ equal to $\Delta_{diss}H^o_m$ ($500H_2O$, 298.15 K) = 17.560 ± 0.024 kJ · mol^{-1} after correction, recommended by the National Bureau of Standards (NBS) [15] to $m = 0.111$ mol · kg^{-1}, which is in very good agreement with the value recommended by the NBS [15,16]: $\Delta_{diss}H^o_m$ ($1000H_2O$, 298.15 K) = 17.584 ± 0.017 kJ · mol^{-1}. The measured value corresponds to an enthalpy at infinite dilution of $\Delta_{diss}H^o_m$ (∞H_2O, 298.15 K) = 17.217 ± 0.024 kJ · mol^{-1}, in good agreement with the NBS data in refs [15] and [16], $\Delta_{diss}H^o_m$ (∞H_2O, 298.15 K) = 17.241 ± 0.018 kJ · mol^{-1}, and that in ref [17], i.e. $\Delta_{diss}H^o_m$ (∞H_2O, 298.15 K) = 17.22 kJ · mol^{-1}.

3. Thermodynamic modelling

The thermodynamic modelling assessment of the molten salt system $BaCl_2$-$CeCl_3$ was performed with the CALPHAD method [18] using the FactSage software, Version 8.2 [19]. Both experimental data obtained in this work and reported in the literature were used to adjust the excess parameters of the Gibbs energy functions of the phases present in this system.

3.1. Stoichiometric compounds

The Gibbs energy function for stoichiometric compounds is dependent on the standard enthalpy of formation ($\Delta_f H^o_m(298)$), the standard entropy ($S^o_m(298)$) and the heat capacity ($C_{p,m}(T)$) as shown in Eq. (1).

$$G(T) = \Delta_f H^o_m(298) - S^o_m(298)T + \int_{298}^{T} C_{p,m}(T)dT - T\int_{298}^{T} \frac{C_{p,m}(T)}{T}dT \quad (1)$$

The isobaric heat capacity $C_{p,m}$ is expressed as a polynomial that takes the form of Eq. (2).

$$C_{p,m}(T) = a + bT + cT^2 + dT^{-2} \quad (2)$$

The compounds in the investigated system are two end-members and an intermediate. The thermodynamic data for these are listed in Table 1. The thermodynamic functions used for $CeCl_3$ were selected by Konings and Kovács [8] as the most reliable functions. The thermodynamic functions used for $BaCl_2$ were obtained from the IVTAN thermochemical database [20]. For the heat capacity of the intermediate $Ba_3Ce_2Cl_{12}$, the Neumann-Kopp additive rule was applied in the absence of experimental data. The standard enthalpy of formation was measured in this work using solution calorimetry, and the obtained value was used in the model. The standard entropy was optimized to fit the available phase diagram data [21,22], while still agreeing with the estimated mixing enthalpy obtained in this work, as detailed in Appendix A. $BaCl_2$ has a phase transition at 1198 K from the low-temperature phase α-$BaCl_2$ (orthorhombic, in space group Pmma) to the high-temperature phase β-$BaCl_2$ (cubic, in space group $Fm\bar{3}m$). $CeCl_3$ exhibits no polymorphism, and crystallizes in the hexagonal space group $P6_3/m$.

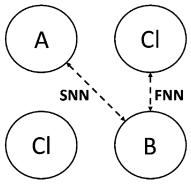

Fig. 1. Schematic representation of a quadruplet in the quadruplet approximation in the quasichemical formalism, indicating what a first-nearest neighbour (FNN) and second-nearest neighbour (SNN) are. A and B are the cations Ba^{2+} and Ce^{3+} respectively.

Table 2
Coordination numbers used in the CALPHAD model of $BaCl_2$–$CeCl_3$ presented in this work.

A	B	$Z^A_{AB/ClCl}$	$Z^B_{AB/ClCl}$	$Z^{Cl}_{AB/ClCl}$
Ba	Ba	6	6	3
Ce	Ce	6	6	2
Ba	Ce	6	3	1.5

3.2. Liquid solution

The excess Gibbs energy terms of the liquid solution are modelled using the quasi-chemical formalism in the quadruplet approximation as proposed by Pelton et al. [23], which has proven to be well-adapted to molten chloride and fluoride salt systems. This description assumes the existence of quadruplets in the liquid, allowing for the modelling of short-range ordering. An example of a quadruplet is given in Fig. 1. This formalism allows for the selection of the composition of maximum short-range ordering through its cation-cation coordination numbers ($Z^{Ba}_{BaCe/ClCl}$ and $Z^{Ce}_{BaCe/ClCl}$), corresponding to the minimum of the Gibbs energy that is most often found near the composition of the lowest eutectic. By fixing these numbers, the anion-anion coordination number is also fixed through Eq. (3), where q_i are the charges of the respective ions. The cation-cation coordination numbers used in this work are given in Table 2.

$$\frac{q_{Ba}}{Z^{Ba}_{BaCe/ClCl}} + \frac{q_{Ce}}{Z^{Ce}_{BaCe/ClCl}} = 2 \cdot \frac{q_{Cl}}{Z^{Cl}_{BaCe/ClCl}} \quad (3)$$

The excess parameters that are optimized are those related to the second-nearest neighbour exchange reaction as given in Eq. (4), where the associated change in Gibbs energy is expressed as Eq. (5).

$$(Ba\text{–}Cl\text{–}Ba) + (Ce\text{–}Cl\text{–}Ce) \longrightarrow 2(Ba\text{–}Cl\text{–}Ce)\Delta g_{BaCe/ClCl} \quad (4)$$

$$\Delta g_{BaCe/ClCl} = \Delta g^0_{BaCe/ClCl} + \Sigma_{i\geq 1} g^{i0}_{BaCe/ClCl}\chi^i_{BaCe/ClCl} + \Sigma_{j\geq 1} g^{0j}_{BaCe/ClCl}\chi^j_{CeBa/ClCl} \quad (5)$$

In Eq. (5) the terms $\Delta g^0_{BaCe/ClCl}$, $g^{i0}_{BaCe/ClCl}$ and $g^{0j}_{BaCe/ClCl}$ are composition-independent coefficients that may depend on temperature. The composition dependence of the Gibbs energy is apparent through $\chi_{BaCe/ClCl}$ as these are defined as per Eq. (6). In this equation X_{AA} is

the cation-cation pair fraction, or the molar fraction of the quadruplet containing two cations A. For this binary system, $\{X_{AA} + X_{AB} + X_{BB}\}$ is equal to one.

$$\chi_{AB/ClCl} = \frac{X_{AA}}{X_{AA} + X_{AB} + X_{BB}} \tag{6}$$

The Gibbs energy function used in this work to describe the liquid solution is given in Eq. (7).

$$\Delta g_{BaCe/ClCl} = -8250 - 3T + \chi_{BaCe/ClCl}(1500) + \chi_{CeBa/ClCl}(-2000 + 8.8T) + \chi^2_{CeBa/ClCl}(-3T) \tag{7}$$

3.3. Solid solution modelling

The thermodynamic description of solid-solutions is done using the two-sublattice polynomial model, consistent with the description used in the JRC Molten Salt Database (JRCMSD) [24]. The Gibbs energy function of the solid-solution is given in Eq. (8).

$$G(T) = X_A \cdot G^0_A + X_B \cdot G^0_B + X_A RT lnX_A + X_B RT lnX_B + \Delta G^{excess}_m \tag{8}$$

In the above equation, G^0_i are the end-member molar Gibbs energies, and X_i are the site molar fractions of the end-members $BaCl_2$ (A) and $CeCl_3$ (B). The third and fourth terms in Eq. (8) represent the configurational entropy. The excess Gibbs energy, presented in Eq. (8) as ΔG^{excess}_m, is defined as in Eq. (9).

$$\Delta G^{excess}_m = \Sigma_{i,j\geq 1} y^i_A y^i_B L^{ij}_{AB} \tag{9}$$

The term L^{ij}_{AB} in Eq. (9) is an interaction coefficient that can be a function of temperature if necessary. The equivalent site fractions y_A and y_B are charge equivalent site fractions. In this work, these fractions are y_{Ba} and y_{Ce}, as defined by Eq. (10) and Eq. (11)

$$y_{Ba} = \frac{2X_{Ba}}{2X_{Ba} + 3X_{Ce}} \tag{10}$$

$$y_{Ce} = \frac{3X_{Ce}}{3X_{Ce} + 2X_{Ba}} \tag{11}$$

The Gibbs energy function used in this work to describe the solid solution is given in Eq. (12).

$$\Delta G^{excess}_m = y_{Ba}y_{Ce}(-11400 + 3T) + y^2_{Ba}y_{Ce}(-4400 + 2T) + y_{Ba}y^2_{Ce}(21000 - 10T) \tag{12}$$

4. Literature review

The data reported in the literature on the $BaCl_2$–$CeCl_3$ system includes phase diagram information and structural studies of the intermediate compound.

The phase diagram of the molten salt system $BaCl_2$–$CeCl_3$ has been studied by Morozov et al. using thermal analysis [21]. Their work is shown in Fig. 2. Morozov et al. reported a single eutectic system with one intermediate compound of composition Ba_3CeCl_9. The existence of the intermediate Ba_3CeCl_9 has not been reported elsewhere. However, another structure containing both barium, cerium and chloride was reported by Meyer et al. [25] as $Ba_9Ce_6Cl_{34}O$. Meyer et al. reported the $Ba_9Ce_6Cl_{34}X$ composition based on X-ray powder diffraction, with X corresponding to a space for an interstitial atom. From an electroneutrality perspective, Meyer et al. argued that this must be an oxygen anion, though they mentioned that a chloride ion would be more feasible considering the size of the hole. We suspect that there are in fact two chloride anions present in the structure, satisfying the electroneutrality condition, rather than one oxygen anion, corresponding to the chemical formula $Ba_3Ce_2Cl_{12}$ ($x_{CeCl_3} = 0.4$). Gauging the invariant points presented in the phase diagram of Morozov et al., it is not unlikely that this is indeed the intermediate they observe, as they do not measure the

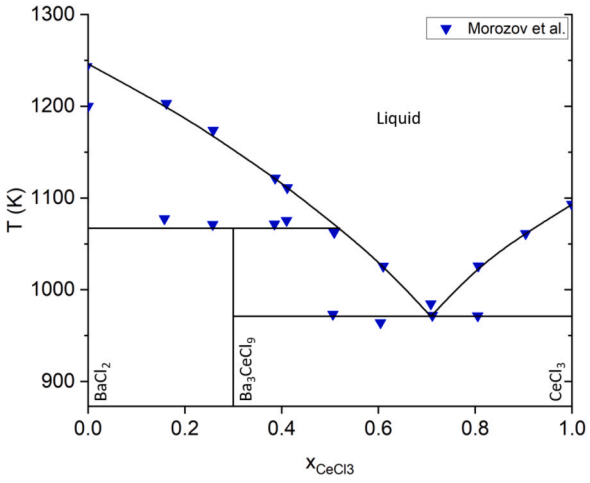

Fig. 2. Measured invariant points in the $BaCl_2$–$CeCl_3$ system reported by Morozov et al. [21], phase diagram re-sketched from the original figure published. The existence of intermediate Ba_3CeCl_9 was suggested by the original authors.

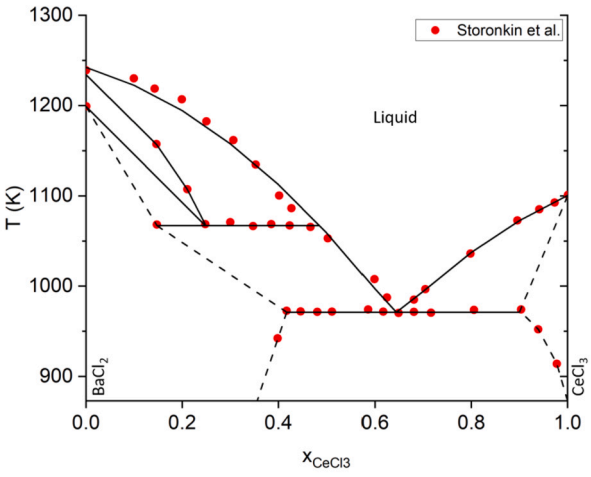

Fig. 3. Measured invariant points in the $BaCl_2$–$CeCl_3$ system reported by Storonkin et al. [22], phase diagram re-sketched from the original figure published. Dashed lines correspond to solid solutions as identified by the original authors.

equilibrium event at T = 973 K (700 °C) at compositions $x_{CeCl_3} \leq 0.4$, which indicates a possible intermediate at this composition. This system was also investigated by Storonkin et al. using a thermographic method [22]. Their data are shown in Fig. 3, and they postulate that there may be solid solutions existing at compositions near $BaCl_2$ and $CeCl_3$.

Based on the experimental data of Morozov et al. as shown in Fig. 2, Zhang et al. [26] performed a thermodynamic modelling assessment, using the quasi-chemical formalism in the pair approximation. The authors included the Ba_3CeCl_9 intermediate, although its existence is not supported by crystal data in the literature. No solid solubility on the $BaCl_2$-rich or $CeCl_3$-rich sides was reported either. Their calculation of the mixing enthalpy of the molten salt system is moreover based solely on their thermodynamic model, and has not been fitted to experimental or estimated mixing enthalpy data. Their calculated values are slightly more negative (minima of $-7400\ J \cdot mol^{-1}$ versus $-5800\ J \cdot mol^{-1}$) than those obtained in this work using Davis' method of estimation [27], as described in detail in Appendix A. It is also worth mentioning that the composition of the minimum value in the model of Zhang et al. is at $x_{CeCl3} = 0.5$, while the minimum determined using Davis' method is at $x_{CeCl3} = 0.7$, again indicating a slight difference. In view of the dis-

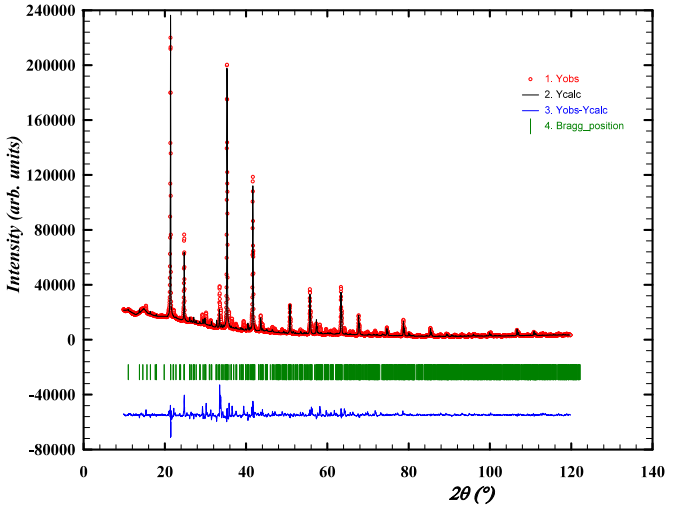

Fig. 4. Profile refinement [9] of X-ray diffraction data using the crystal structure of $Ba_9Ce_6Cl_{34}O$ as reported by Meyer et al. [25] as structural model. The observed intensity (Yobs, red) is plotted along with the calculated intensity from the refinement (Ycalc, black), and the difference between the two is shown (Yobs-Ycalc, blue). The angles at which reflections occur are shown as well (Bragg positions, vertical lines). Measurement at λ = Cu-Kα.

crepancies noticed in the literature on this system, both experimental data and modelling assessment were revisited in this work.

5. Results and discussion

The $BaCl_2$-$CeCl_3$ binary system has been investigated experimentally through the use of XRD, ND, quenching experiments and DSC. The mixing enthalpy of this system has been estimated in the absence of literature data on this property. The reader is referred to Appendix A for a detailed explanation of the estimations made for the mixing enthalpy.

5.1. The intermediate $Ba_3Ce_2Cl_{12}$

The existence of an intermediate in the $BaCl_2$-$CeCl_3$ system at a composition of $x_{CeCl_3} = 0.4$ can be suspected from the experimental data on phase transitions from Morozov et al. [21]. However, there are no intermediate salts known of composition $Ba_3Ce_2Cl_{12}$ in the literature. Meyer et al. [25] did suggest the existence of $Ba_9Ce_6Cl_{34}O$ as discussed in Section 4, which has the same stoichiometric ratio of barium to cerium. There is still debate about the existence and stoichiometry of this intermediate, as Meyer et al. suggest it contains oxygen. The crystal structure was determined using X-ray powder diffraction to be tetragonal, in space group I4/m (87), with cell parameters a,b = 11.348(3) Å and c = 21.729(5) Å. Our work, as detailed hereafter, suggests to discard the presence of oxygen in this structure, and instead suggests the presence of two chlorine ions, which also satisfies the charge condition.

In order to investigate this intermediate, a synthesis was performed as described in Section 2.1 using a solid state route. The synthesised material was subsequently investigated using XRD and ND, and the profile refinements of this material are shown in Fig. 4 (XRD) and Fig. 5 (ND), respectively. For this refinement, the structure of $Ba_9Ce_6Cl_{34}O$ as identified by Meyer et al. was used as a starting structural model. The oxygen ion they suggest to balance the charge is not present in the crystallographic data they report. The refinements performed here also lack two chlorine atoms.

The profile refinements in Figs. 4 and 5 show good agreement between the observed and the calculated patterns, indicating that the synthesis was a success. The refined crystal structure of this salt, however, does not account for the presence of oxygen, as seen in Table 3, where the atomic positions refined from the ND data are reported.

Table 3
Refined atomic positions of the crystal structure of $Ba_9Ce_6Cl_{34}X$ as calculated with a profile refinement of the ND spectrum. The number between brackets is the error on the last digit. χ^2 = 67.9, R_{wp} = 28.3, R_{exp} = 3.43.

Site	Element	Wyckoff Index	x	y	z
Cl1	Cl	16i	0.035(2)	0.178(2)	0.383(1)
Ba1	Ba	16i	0.111(3)	0.295(3)	0.139(1)
Cl2	Cl	16i	0.212(2)	0.112(2)	0.241(1)
Cl3	Cl	16i	0.208(3)	0.077(3)	0.072(1)
Cl4	Cl	8h	0.206(2)	0.401(2)	0
Ce1	Ce	8h	0.394(5)	0.212(4)	0
Cl5	Cl	8g	0	0.5	0.080(1)
Ce2	Ce	4e	0	0	0.868(3)
Cl6	Cl	4d	0	0.5	0.25
Ba2	Ba	2a	0	0	0

Table 4
Comparison between cell parameters as obtained from XRD and ND refinements with that obtained by Meyer et al. [25].

Source	a,b (Å)	c (Å)
Meyer et al. [25]	11.348(3)	21.729(5)
XRD refinement	11.357(2)	21.535(8)
ND refinement	11.336(9)	21.529(36)

A comparison between the lattice parameters proposed by Meyer et al., the refinement of the XRD pattern and the refinement of the ND pattern is given in Table 4. No large discrepancies were observed that would suggest a vastly different crystal structure from what Meyer et al. report. However, the profile matching between experimental data and the fitted model is not fully ideal, as evidenced by the ND data. This suggests that the crystal structure of $Ba_9Ce_6Cl_{36}$ (or $Ba_3Ce_2Cl_{12}$) as hypothesied herein should be revisited.

5.2. Solid-solutions - $BaCl_2$-rich side

The existence and structural parameters of solid-solutions in this binary system have been investigated through the use of quenching experiments followed by XRD. The compositions at which quenching experiments were performed are x_{CeCl3} = [0.05, 0.075, 0.15, 0.2, 0.3], quenched from T = 1025 K, and $x_{CeCl3} = 0.1$, quenched from 1275 K.

A defining characteristic of the solid-solution under investigation is the fact that the structure is identical to the high-temperature structure of $BaCl_2$, β-$BaCl_2$, albeit with a shift in cell parameters. This shift is due to the insertion of the smaller Ce^{3+} cation ($R_{crystal}$ = 1.15 Å [28]) instead of the larger Ba^{2+} ($R_{crystal}$ = 1.49 Å [28]) cation in the crystal structure of β-$BaCl_2$. This structure is a fluorite structure with space group $Fm\bar{3}m$ (225). The refinement of lattice parameters shows an excellent agreement between the measured and calculated pattern, as exemplified in Fig. 6 for the $x_{CeCl3} = 0.1$ composition. The occupancies of the shared Ba^{2+}-Ce^{3+} atomic positions are not refined.

The refined lattice parameters are plotted as a function of composition in Fig. 6, and are listed in Table 5. A decreasing linear trend described with Eq. (13), where V_0 is the volume of β-$BaCl_2$, appears in the single-phase solid-solution cell parameters with increase in $CeCl_3$ content, related to the insertion of the smaller Ce^{3+} cation in the $BaCl_2$ structure. Quenching experiments at x_{CeCl_3} = [0.05, 0.075, 0.3] resulted in a mixture of phases. The first two compositions showed a mixture of solid-solution and α-$BaCl_2$, while the latter composition gave a mixture of solid-solution and $Ba_3Ce_2Cl_{12}$.

$$V(x) = V_0 - 59.51x \tag{13}$$

The data at x_{CeCl_3} = 0.05 and 0.075 in Fig. 7 result in approximately the same cell parameters, suggesting that the composition of the solid

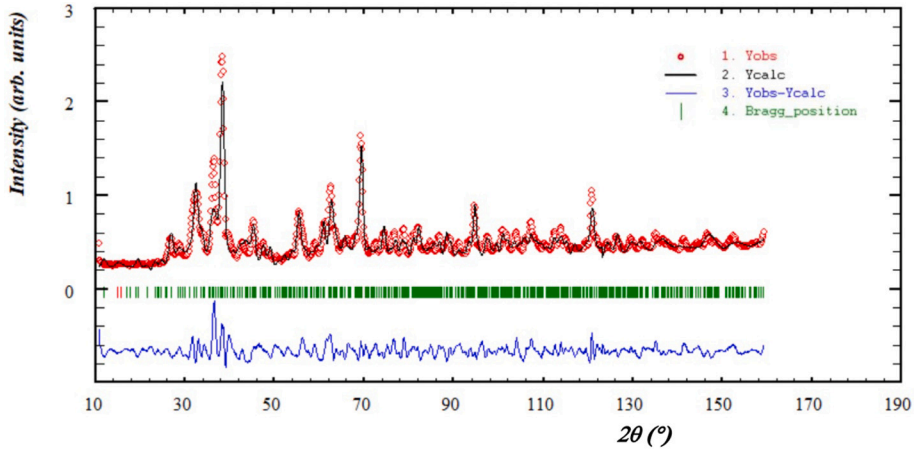

Fig. 5. Profile refinement of the neutron diffraction data. The observed intensity (red circles) is plotted along with the calculated intensity from the refinement (black line), and the difference between the two is shown (blue line). Bragg positions at which reflections occur are also shown (green lines). Measurement at λ = 1.667 Å.

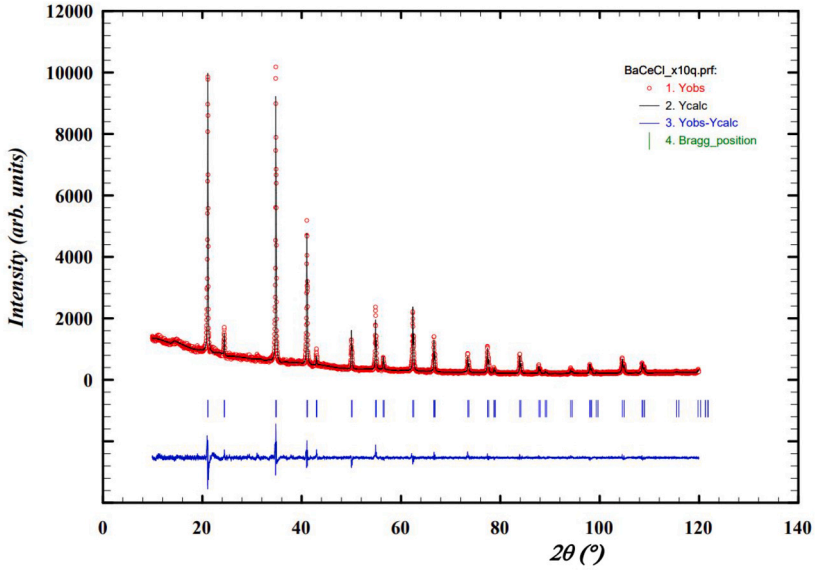

Fig. 6. Profile refinement of a quenched sample with $x_{CeCl3} = 0.1$, with a fully formed cubic solid-solution ($Ba_{1-x}Ce_xCl_{x+2}$ (cub)). This particular sample was quenched from 1275 K. The observed intensity (Yobs, red) is plotted along with the calculated intensity from the refinement (Ycalc, black), and the difference between the two is shown (Yobs-Ycalc, blue). The angles at which reflections occur are shown as well (Bragg positions, vertical lines). Measurement at λ = Cu-Kα.

Table 5
Refined cell parameters of the XRD spectra of samples containing solid solutions on the $BaCl_2$-rich side, as well as the refined cell parameters of the solid solution.

x_{CeCl3}	a, b, c (Å)	V (Å^3)	Weight fraction solid-solution (%)	Second phase
0	7.3240(5)	392.86(8)	0	$BaCl_2$
0.05	7.2656(5)	383.54(8)	72.57	α-$BaCl_2$
0.075	7.2668(5)	383.73(8)	57.48	α-$BaCl_2$
0.1	7.2869(5)	386.93(8)	100	none
0.15	7.2639(5)	383.27(8)	100	none
0.2	7.2524(6)	381.46(9)	100	none
0.3	7.2405(5)	379.58(8)	36.25	$Ba_3Ce_2Cl_{12}$

solution that is formed contains approximately 18% $CeCl_3$, obtained from the linear fit in Fig. 7. This is an indication that the solid solution at this temperature has a minimum solubility of 18% $CeCl_3$ at T = 1023 K. The result of the measurement at $x_{CeCl_3} = 0.3$ would indicate a solid-solution containing approximately 24.5% percent $CeCl_3$, indicating the maximum solubility at this temperature. For the three mentioned compositions, the resulting XRD showed a mixture of phases, which was not the case for other measurements. For each of these refinements, the weight fraction of each phase present was also calculated with the profile refinement. From these weight fractions, the cerium-content in the solid-solution was derived, and the result is shown in Table 6. The agreement with the data extrapolated from the linear fit in Fig. 7 is good, given the uncertainties on both methods. The observed solid solution is largely in agreement with the work of Storonkin et al. [22], shown in Fig. 3. The difference is that the solid solution was only observed at elevated temperatures in this work, while the phase diagram by Storonkin et al. suggests stability at room temperature.

5.3. Solid-solutions - $CeCl_3$-rich side

In addition to the solid solution on the $BaCl_2$-rich side of the phase diagram, experimental data obtained in this work as well as that of Storonkin et al. indicate that a solid solution could be present at the $CeCl_3$-rich side of the phase diagram. Structurally, this solid solution differs from the solid solution at the $BaCl_2$-rich side ($Ba_{1-x}Ce_xCl_{2+x}$ (cub)) in that it has an hexagonal crystal structure ($Ba_{1-y}Ce_yCl_{2+y}$

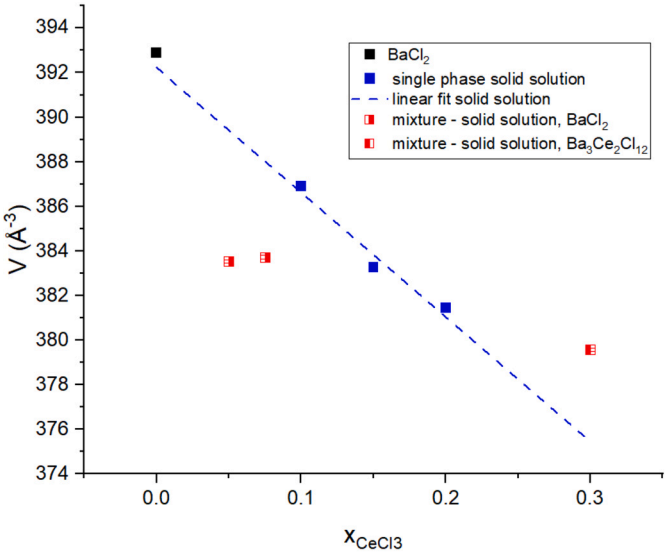

Fig. 7. Evolution of the cell volume of the measured single-phase solid-solution as a function of the nominal $CeCl_3$ molar fraction. The blue dashed line is a linear fit through the single-phase results. Data for $x_{CeCl_3} = 0.1$ has been obtained at a different temperature (1273 K) than the other experiments (1023 K). $BaCl_2$ as listed in the legend is the cubic β-$BaCl_2$ phase.

Table 6
Cerium-fractions in the solid solutions $Ba_{1-x}Ce_xCl_{2+x}$ estimated using the linear trend obtained from Fig. 7 and as calculated from the weight fractions (profile refinements).

x_{CeCl_3}	$x^{cell\,parameter}_{CeCl_3,ss}$ linear trend	$x^{weight\,fraction}_{CeCl_3,ss}$ profile refinements
0.05	0.187	0.155
0.075	0.180	0.152
0.30	0.245	0.226

(hex)). Quenching experiments were performed to investigate the presence and possible stability of this solid solution at elevated temperatures. Compositions that were investigated are x_{CeCl_3} = [0.95, 0.975, 0.99], quenched to room temperature from 973 K, and $x_{CeCl3} = 0.9$, quenched from 1023 K. These mixtures were investigated using post-quenching XRD, and profile refinements were performed, which are available as supplementary material. An example of these refinements is given in Fig. 8 for the composition $x_{CeCl3} = 0.95$, indicating a mixture of $Ba_3Ce_2Cl_{12}$ and solid-solution.

At the $CeCl_3$-rich side of the phase diagram, Ba^{2+} ions are inserted in the crystal structure of $CeCl_3$, which is hexagonal in space group $P6_3/m$ 176. The refined cell parameters of these mixtures are reported in Table 7 and are shown in Fig. 9.

The cell volumes presented in Fig. 9 display a minor increase of the cell parameters with increasing $BaCl_2$-content in the sample, which suggests the formation of a solid solution. The linear fit of this solid solution is described by Eq. (14), with V_0 the volume of $CeCl_3$.

$$V(x) = V_0 - 4.671(1 - x) \tag{14}$$

5.4. Standard enthalpy of formation determination

The standard enthalpy of formation of $Ba_3Ce_2Cl_{12}$ was measured using the thermochemical cycles shown in Table 8 in 25 mL H_2O. The dissolution reactions reported in Eqs. (15) and (16) were performed successively. The amounts of $Ba_3Ce_2Cl_{12}$ and {$BaCl_2$ + $CeCl_3$} were

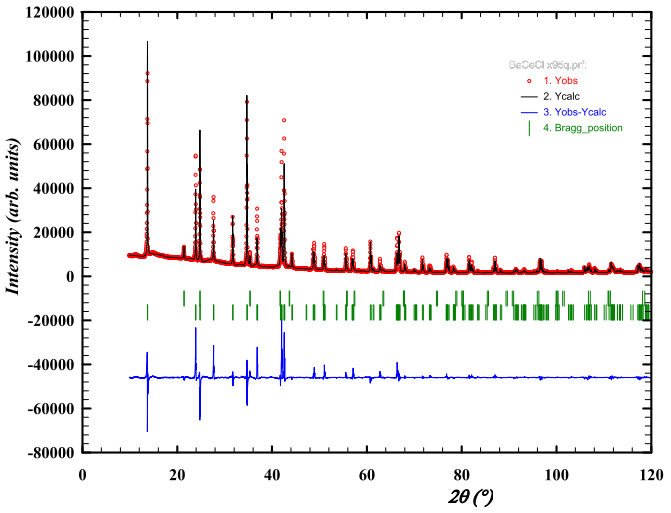

Fig. 8. Profile refinement of a quenched sample of composition $x_{CeCl_3} = 0.95$ to investigate the existence of a solid solution. The observed intensity (Yobs, red) is plotted along with the calculated intensity from the refinement (Ycalc, black), and the difference between the two is shown (Yobs-Ycalc, blue). The angles at which reflections occur are shown as well (Bragg positions, vertical lines). Measurement at λ = Cu-Kα.

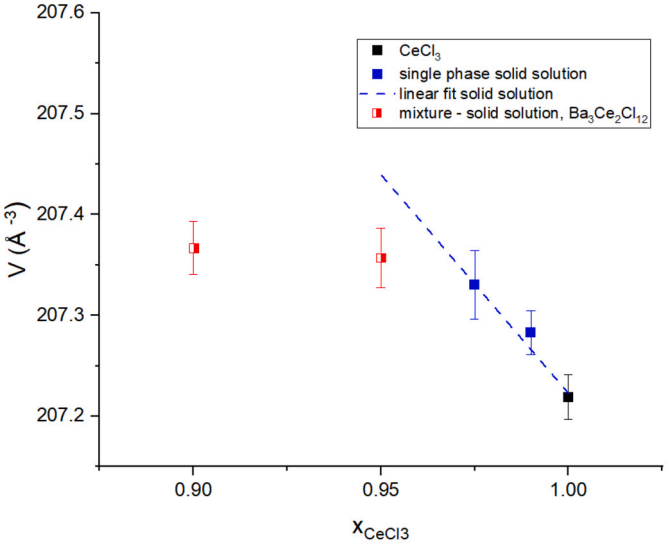

Fig. 9. Refined cell volume as calculated with profile refinements performed in this work. An increasing linear trend is apparent, following the insertion of the larger Ba^{2+} into the $CeCl_3$ structure. The lattice parameters for $CeCl_3$ were also obtained using a profile refinement.

adjusted so that the solutions obtained as products of reactions (15) and (16) had the same final concentrations of dissolved ions.

$$Ba_3Ce_2Cl_{12}(cr) + H_2O(l) = 3BaCl_2(sln) + 2CeCl_3(sln) \qquad \Delta_{sln}H_1 \tag{15}$$

$$3BaCl_2(cr) + 2CeCl_3(cr) + H_2O(l) = 3BaCl_2(sln) + 2CeCl_3(sln) \qquad \Delta_{sln}H_2 \tag{16}$$

The dissolution of the salts $BaCl_2$, $CeCl_3$ and $Ba_3Ce_2Cl_{12}$ was in all cases instantaneous. The details of the calorimetric results are given in Table 9. The enthalpy of the formation reaction from the constituting binary chloride salts can be expressed as in Eq (17). The standard enthalpy of formation has been calculated using Equation (18). The obtained value for the standard enthalpy of formation of $Ba_3Ce_2Cl_{12}$ is -4711.7 ± 6.0 kJ · mol^{-1}.

Table 7
Refined cell parameters of the XRD spectra of samples containing solid solutions on the $CeCl_3$-rich side, as well as the refined cell parameters of $CeCl_3$.

x_{CeCl3}	a, b (Å)	c (Å)	V (Å^3)	Weight fraction solid solution (%)	Second phase
1	7.4428(3)	4.3194(3)	207.22(2)	0	$CeCl_3$
0.99	7.4439(3)	4.3195(3)	207.28(2)	100	none
0.975	7.4446(5)	4.3197(4)	207.33(3)	100	none
0.95	7.4449(4)	4.3198(4)	207.36(2)	96.26	$Ba_3Ce_2Cl_{12}$
0.9	7.4453(4)	4.3197(3)	207.37(0)	86.89	$Ba_3Ce_2Cl_{12}$

Table 8
Thermochemical cycle used to determine the standard enthalpy of formation of $Ba_3Ce_2Cl_{12}$. Measurements performed in the temperature interval T = 298.15 ± 0.3 K. The enthalpy of formation of $Ba_3Ce_2Cl_{12}$ was calculated using the relation $\Delta_f H^o_m(5) = -\Delta_{sln}H(1) + \Delta_{sln}H(2) + 3\Delta_f H^o_m(3) + 2\Delta_f H^o_m(4)$.

entry	reaction	$\Delta_{sln}H(298.15K)$ (kJ · mol^{-1})	source
1	$Ba_3Ce_2Cl_{12}$ (cr) + H_2O = 3 $BaCl_2$(sln) + 2 $CeCl_3$(sln)	−290.19 ± 0.62[a]	this work
2	3 $BaCl_2$ (cr) + 2 $CeCl_3$ (cr) + H_2O = 3 $BaCl_2$(sln) + 2 $CeCl_3$(sln)	−316.93 ± 0.80[a]	this work

entry	reaction	$\Delta_f H^o_m(298.15K)$ (kJ · mol^{-1})	source
3	Ba(cr) + Cl_2(g) = $BaCl_2$(cr)	−855.2 ± 1.7	[7]
4	Ce(cr) + 3/2 Cl_2(g) = $CeCl_3$(cr)	−1059.7 ± 1.5	[8]
5	3 Ba(cr) + 2 Ce(cr) + 6 Cl_2(g) = $Ba_3Ce_2Cl_{12}$(cr)	−4711.7 ± 6.0	this work

[a] Expanded uncertainty U with a coverage factor $k = 2$, corresponding to a 95% confidence interval.

Table 9
Measured dissolution enthalpies at 298.15 K for $Ba_3Ce_2Cl_{12}$(cr) (M = 1117.65 g · mol^{-1}) in 25 mL H_2O.

entry	m($Ba_3Ce_2Cl_{12}$) (mg)	ΔT (mK)	C_p (J · K^{-1})	Q (J)	$\Delta_r H^o_m$(298.15 K) (kJ · mol^{-1})
1	56.00	162.420	117.683	−14.552	−290.453
2	56.05	121.729	117.691	−14.542	−289.968
3	55.71	121.309	117.345	−14.449	−289.882

entry	m($BaCl_2$ + $CeCl_3$) (mg)	ΔT (mK)	C_p (J · K^{-1})	Q (J)	$\Delta_r H^o_m$(298.15 K) (kJ · mol^{-1})
1	31.79 + 25.37	129.699	117.823	−16.157	−317.430
2	31.40 + 25.56	128.567	117.065	−16.763	−316.424
3	30.83 + 24.40	133.421	117.469	15.673	−317.026

$$\Delta_r H^o_m = -\Delta_{sln}H_1 + \Delta_{sln}H_2 \quad (17)$$

$$\Delta_f H^o_m(5) = -\Delta_{sln}H(1) + \Delta_{sln}H(2) + 3\Delta_f H^o_m(3) + 2\Delta_f H^o_m(4) \quad (18)$$

5.5. Phase equilibria measurements using DSC

A list of mixtures measured in this work by DSC, along with the temperatures of invariant transitions and associated invariant reactions, is presented in Table 10. The phase equilibria are also shown on the optimized phase diagram in Fig. 10.

5.6. Thermodynamic model

With the thermodynamic descriptions of the parameters in the system as described in Table 1, Eq. (7) and Eq. (12), the phase diagram and mixing enthalpy of the system were calculated. The phase diagram is shown in Fig. 10, and the enthalpy of mixing is reported in Fig. 11. The invariant equilibria calculated with this CALPHAD model are presented in Table 11.

The CALPHAD model displayed in Fig. 10 shows good agreement with the measured invariant points. Fig. 11 shows that the calculated mixing enthalpy also reproduces the mixing enthalpy as estimated with Davis' method well. A few differences between the data obtained in this work and the phase equilibria as interpreted by Morozov et al. [21] and Storonkin et al. [22] are worth pointing out. First, the liquidus that is measured here is rather flat between the compositions $x_{CeCl_3} = 0.025$ and $x_{CeCl_3} = 0.3$. This could be related to the formation of a solid-solution in this composition range, as the equilibrium between $Ba_{1-x}Ce_xCl_{2+x}$ and {$Ba_{1-x}Ce_xCl_{2+x}$ + L} is not observable. Also in this composition range, thermal events were detected around T = 950 K in contrast to the previous works, which according to the present model, correspond to the formation of this solid solution. The peritectic decomposition of the intermediate $Ba_3Ce_2Cl_{12}$ observed near T = 1100 K is also reported in the literature, though Morozov et al. identified this intermediate as Ba_3CeCl_9. The eutectic composition that was measured in this work ($x_{CeCl3} = 0.67$) is approximately at the same composition as measured by Morozov et al. ($x_{CeCl3} = 0.68$) and Storonkin et al. ($x_{CeCl3} = 0.65$). Finally, Storonkin et al. observed a solid-solution on the $CeCl_3$-rich side of the phase diagram, and the DSC data obtained in this work corroborates that. The solubility limit of $BaCl_2$ in $CeCl_3$ is around 5% at temperatures above 970 K, while that of $CeCl_3$ in $BaCl_2$ has a maximum of about 25% at 1060 K.

5.7. Ternary extrapolation

As mentioned in the introduction, Ce is sometimes used as a simulant for Pu, which is especially helpful when investigating higher order systems such as NaCl–$BaCl_2$–$PuCl_3$. To investigate the effect of $BaCl_2$ addition on the melting properties of the NaCl–$PuCl_3$ fuel, a thermodynamic model of the system NaCl–$BaCl_2$–$CeCl_3$ was constructed, using the model by Chartrand et al. [29] for the NaCl–$BaCl_2$ system, and the work of Lu et al. [30] for the NaCl–$CeCl_3$ system. This extrapolation to the ternary system is solely based on the constituting binary systems, and no ternary excess terms were added.

Table 10
Equilibrium data in the $BaCl_2$–$CeCl_3$ system as measured by DSC.

x_{CeCl_3} [a]	T (K)[b]	Equilibrium	Equilibrium reaction
0	1197	α-β transition	α-$BaCl_2 = \beta$-$BaCl_2$
	1235	Congruent melting	β-$BaCl_2$ = L
0.024	1164	Unknown	-
	1196	Solidus	α-$BaCl_2$+ $Ba_{1-x}Ce_xCl_{2+x} = Ba_{1-x}Ce_xCl_{2+x}$
	1237	Liquidus	$Ba_{1-x}Ce_xCl_{2+x}$ = L
0.037	1176	Solidus	α-$BaCl_2$ + $Ba_{1-x}Ce_xCl_{2+x} = Ba_{1-x}Ce_xCl_{2+x}$
	1235	Liquidus	$Ba_{1-x}Ce_xCl_{2+x}$ + L' = L
0.060	952	Eutectoid	α-$BaCl_2$ + $Ba_3Ce_2Cl_{12} = Ba_{1-x}Ce_xCl_{2+x}$
	1147	Solidus	α-$BaCl_2$ + $Ba_{1-x}Ce_xCl_{2+x} = Ba_{1-x}Ce_xCl_{2+x}$
	1239	Liquidus	$Ba_{1-x}Ce_xCl_{2+x}$ + L' = L
0.075	943	Eutectoid	α-$BaCl_2$ + $Ba_3Ce_2Cl_{12} = Ba_{1-x}Ce_xCl_{2+x}$
	1235	Liquidus	$Ba_{1-x}Ce_xCl_{2+x}$ + L' = L
0.098	944	Eutectoid	α-$BaCl_2$ + $Ba_3Ce_2Cl_{12} = Ba_{1-x}Ce_xCl_{2+x}$
	1236	Liquidus	$Ba_{1-x}Ce_xCl_{2+x}$ + L' = L
0.126	943	Eutectoid	α-$BaCl_2$ + $Ba_3Ce_2Cl_{12} = Ba_{1-x}Ce_xCl_{2+x}$
	1235	Liquidus	$Ba_{1-x}Ce_xCl_{2+x}$ + L' = L
0.170	944	Eutectoid	α-$BaCl_2$ + $Ba_3Ce_2Cl_{12} = Ba_{1-x}Ce_xCl_{2+x}$
	966	Unknown	-
	1233	Liquidus	$Ba_{1-x}Ce_xCl_{2+x}$ + L' = L
0.175	943	Eutectoid	α-$BaCl_2$ + $Ba_3Ce_2Cl_{12} = Ba_{1-x}Ce_xCl_{2+x}$
	1197	Unknown	-
	1225	Liquidus	$Ba_{1-x}Ce_xCl_{2+x}$ + L' = L
0.199	1217	Liquidus	$Ba_{1-x}Ce_xCl_{2+x}$ + L' = L
0.200	945	Eutectoid	α-$BaCl_2$ + $Ba_3Ce_2Cl_{12} = Ba_{1-x}Ce_xCl_{2+x}$
	1064	Unknown	-
	1233	Liquidus	$Ba_{1-x}Ce_xCl_{2+x}$ + L' = L
0.249	944	Eutectoid	α-$BaCl_2$ + $Ba_3Ce_2Cl_{12} = Ba_{1-x}Ce_xCl_{2+x}$
	1082	Solidus	$Ba_{1-x}Ce_xCl_{2+x} = Ba_{1-x}Ce_xCl_{2+x}$ + L'
	1227	Liquidus	$Ba_{1-x}Ce_xCl_{2+x}$ + L' = L
0.278	1057	Peritectic	$Ba_3Ce_2Cl_{12} = Ba_{1-x}Ce_xCl_{2+x}$ + L'
	1174	Liquidus	$Ba_{1-x}Ce_xCl_{2+x}$ + L' = L
0.3	1066	Peritectic	$Ba_3Ce_2Cl_{12} = Ba_{1-x}Ce_xCl_{2+x}$ + L'
	1163	Liquidus	$Ba_{1-x}Ce_xCl_{2+x}$ + L' = L
0.336	1069	Peritectic	$Ba_3Ce_2Cl_{12} = Ba_{1-x}Ce_xCl_{2+x}$ + L'
	1139	Liquidus	$Ba_{1-x}Ce_xCl_{2+x}$ + L' = L
0.347	1053	Unknown	-
	1072	Peritectic	$Ba_3Ce_2Cl_{12} = Ba_{1-x}Ce_xCl_{2+x}$ + L'
	1113	Liquidus	$Ba_{1-x}Ce_xCl_{2+x}$ + L' = L
0.39	1052	Unknown	
	1077	Peritectic	$Ba_3Ce_2Cl_{12} = Ba_{1-x}Ce_xCl_{2+x}$ + L'
0.4	960	Eutectic	$Ce_{1-y}Ba_yCl_{3-y}$ + $Ba_3Ce_2Cl_{12}$ = L
	1062	Peritectic	$Ba_3Ce_2Cl_{12} = Ba_{1-x}Ce_xCl_{2+x}$ + L'
	1080	Liquidus	$Ba_{1-x}Ce_xCl_{2+x}$ + L' = L
0.444	942	Eutectic	$Ce_{1-y}Ba_yCl_{3-y}$ + $Ba_3Ce_2Cl_{12}$ = L
	1043	Unknown	-
	1067	Liquidus	$Ba_3Ce_2Cl_{12}$ + L' = L
0.5	962	Unknown	-
	965	Eutectic	$Ce_{1-y}Ba_yCl_{3-y}$ + $Ba_3Ce_2Cl_{12}$ = L
	1058	Liquidus	$Ba_3Ce_2Cl_{12}$ + L' = L
0.573	969	Eutectic	$Ce_{1-y}Ba_yCl_{3-y}$ + $Ba_3Ce_2Cl_{12}$ = L
	1025	Liquidus	$Ba_3Ce_2Cl_{12}$ + L' = L
0.616	975	Eutectic	$Ce_{1-y}Ba_yCl_{3-y}$ + $Ba_3Ce_2Cl_{12}$ = L
	986	Liquidus	$Ba_3Ce_2Cl_{12}$ + L' = L
0.655	979	Liquidus	$Ba_3Ce_2Cl_{12}$ + L' = L
0.699	971	Eutectic	$Ce_{1-y}Ba_yCl_{3-y}$ + $Ba_3Ce_2Cl_{12}$ = L
	1003	Liquidus	$Ce_{1-y}Ba_yCl_{3-y}$ + L' = L
0.779	967	Eutectic	$Ce_{1-y}Ba_yCl_{3-y}$ + $Ba_3Ce_2Cl_{12}$ = L
	1032	Liquidus	$Ce_{1-y}Ba_yCl_{3-y}$ + L' = L
0.905	968	Eutectic	$Ce_{1-y}Ba_yCl_{3-y}$ + $Ba_3Ce_2Cl_{12}$ = L
	1073	Liquidus	$Ce_{1-y}Ba_yCl_{3-y}$ + L' = L
0.95	959	Solidus	$Ba_3Ce_2Cl_{12}$ + $Ce_{1-y}Ba_yCl_{3-y} = Ce_{1-y}Ba_yCl_{3-y}$
	1084	Liquidus	$Ce_{1-y}Ba_yCl_{3-y}$ + L' = L
0.973	946	Solidus	$Ba_3Ce_2Cl_{12}$ + $Ce_{1-y}Ba_yCl_{3-y} = Ce_{1-y}Ba_yCl_{3-y}$
	1089	Liquidus	$Ce_{1-y}Ba_yCl_{3-y}$ + L' = L
1	1087	Congruent melting	$CeCl_3$ = L

[a] The uncertainties on compositions x_{CeCl3} are ±0.005.
[b] The uncertainties on temperatures are ±5 K for pure end-members and ±10 K for mixtures.

In Fig. 12, the pseudo-binary phase diagram between {0.95 NaCl + 0.05 $BaCl_2$} and {0.95 $CeCl_3$ + 0.05 $BaCl_2$} is shown alongside the phase diagram of the system NaCl–$CeCl_3$, in order to show the effect of 5% $BaCl_2$ addition on the melting behaviour of this system. This figure shows that the addition of $BaCl_2$ gives rise to a higher eutectic temperature because of the formation of $Ba_3Ce_2Cl_{12}$ (area F in Fig. 12). This implies that the addition of $BaCl_2$ increases the eutectic temperature and therefore lowers the margin to solidification during reactor

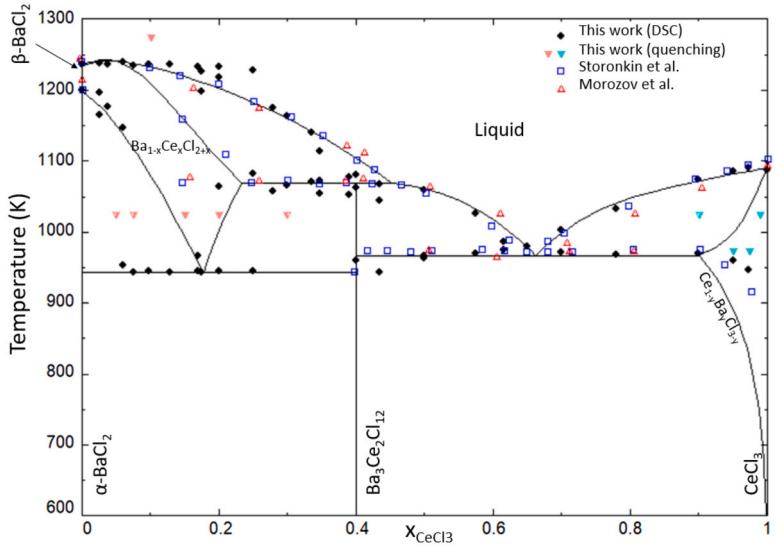

Fig. 10. Phase diagram of the $BaCl_2$-$CeCl_3$ binary system, as calculated with the optimized thermodynamic model. Data from Morozov et al. [21] (empty orange triangles), Storonkin et al. [22] (empty blue squares) and this work (filled black circles). Labels for the quenching experiments are completely filled (pure solid-solution), right-filled (mixture of solid-solution and $BaCl_2$) and left-filled (mixture of solid-solution and $Ba_3Ce_2Cl_{12}$).

Table 11
Calculated invariant equilibria in the $BaCl_2$–$CeCl_3$ system using the model presented in this work (CALPHAD), as well as measured values of these invariants from Morozov et al. [21], Storonkin et al. [22] and this work (DSC).

x_{CeCl3}	T (K)				Equilibrium	Invariant reaction
	CALPHAD	Morozov	Storonkin	This work (DSC)		
0	1198	1200	1199	1197 ± 5	α-β transition	α-$BaCl_2 = \beta$-$BaCl_2$
	1234	1243	1239	1235 ± 5	Congruent melting	β-$BaCl_2 = L$
0.18	940			944 ± 10	Eutectoid	$BaCl_2 + Ba_3Ce_2Cl_{12} = Ba_{1-x}Ce_xCl_{2+x}$
0.4	1068	1071	1069	1062 ± 10	Peritectic	$Ba_3Ce_2Cl_{12} = Ba_{1-x}Ce_xCl_{2+x} + L'$
0.66	966	972	970	971 ± 10	Eutectic	$Ba_3Ce_2Cl_{12} + Ce_{1-y}Ba_yCl_{3-y} = L$
1	1089	1093	1101	1093 ± 5	Congruent melting	$CeCl_3 = L$

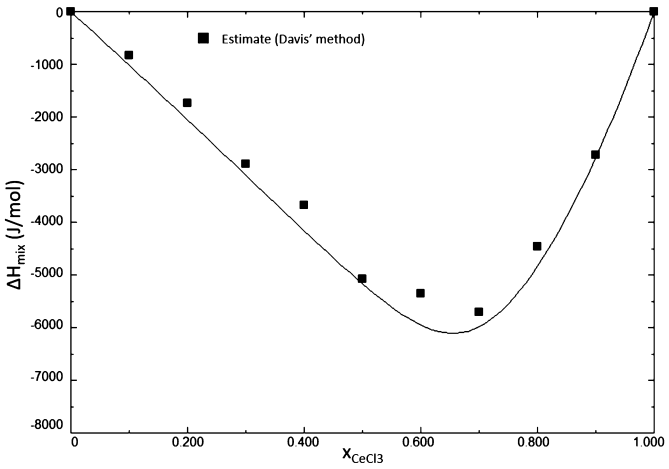

Fig. 11. Mixing enthalpy of the $BaCl_2$-$CeCl_3$ binary system at T = 1250 K, as calculated with the thermodynamic model presented in this section. The mixing enthalpy data were obtained with the mixing enthalpy estimation method presented in Appendix A.

operation, and poses the threat of precipitation of the $PuCl_3$ in the fuel at low temperatures. The effect of 1%, 2%, 3% and 4% $BaCl_2$ additions on this binary system, as well as the liquidus projection of the ternary system, are presented in Appendix B.

6. Summary

A thermodynamic assessment of the molten salt system $BaCl_2$–$CeCl_3$ is presented in this work based on the quasi-chemical formalism in the quadruplet approximation for the liquid solution. This system is characterized by: i) a single eutectic, ii) a peritectic decomposition of the intermediate $Ba_3Ce_2Cl_{12}$, iii) a $Ba_{1-x}Ce_xCl_{2+x}$ (cubic) solid-solution stable at high temperature in the composition range x_{CeCl3} = [0.05-0.25], iv) a $Ce_{1-y}Ba_yCl_{3-y}$ (hexagonal) solid-solution stable at high temperatures in the composition range x_{CeCl3} = [0.925-1]. The structures of the solid-solutions in this system have been characterised using XRD, and the intermediate $Ba_3Ce_2Cl_{12}$ has been characterised with XRD and ND. The mixing enthalpy of this system has been estimated with Davis' method over the entire composition range. Extrapolation to the ternary system NaCl–$BaCl_2$–$CeCl_3$ shows a lowered margin to solidification and precipitate formation upon addition of 5% $BaCl_2$.

CRediT authorship contribution statement

D.C. Alders: Investigation, Writing – original draft, Writing – review & editing. **J. Vlieland:** Investigation. **M. Thijs:** Investigation. **R.J.M. Konings:** Supervision, Writing – review & editing. **A.L. Smith:** Supervision, Writing – original draft, Writing – review & editing.

Declaration of competing interest

The authors declare the following financial interests/personal relationships which may be considered as potential competing interests:

Dennis Alders reports financial support was provided by Orano SA. If there are other authors, they declare that they have no known competing financial interests or personal relationships that could have appeared to influence the work reported in this paper.

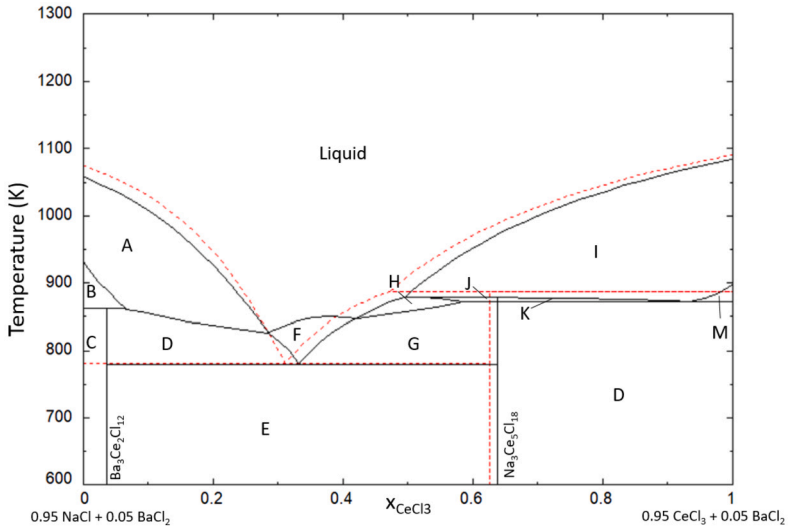

Fig. 12. Phase diagram of the {0.95 NaCl + 0.05 $BaCl_2$}-{0.95 $CeCl_3$ + 0.05 $BaCl_2$} pseudo-binary section of the NaCl–$BaCl_2$–$CeCl_3$ ternary system. The labelled phases are NaCl + L' (A), NaCl + $BaCl_2$ + L' (B), $BaCl_2$ + $Ba_3Ce_2Cl_{12}$ + NaCl (C), NaCl + $Ba_3Ce_2Cl_{12}$ + L' (D), NaCl + $Na_3Ce_5Cl_{18}$ + $Ba_3Ce_2Cl_{12}$ (E), $Ba_3Ce_2Cl_{12}$ + L' (F), $Na_3Ce_5Cl_{18}$ + $Ba_3Ce_2Cl_{12}$ + L' (G), $Na_3Ce_5Cl_{18}$ + L' (H), $Ce_{1-y}Ba_yCl_{3-y}$ + L' (I), $Na_3Ce_5Cl_{18}$ + $Ba_{1-x}Ce_xCl_{2+x}$ + L' (J), $Na_3Ce_5Cl_{18}$ + $Ce_{1-y}Ba_yCl_{3-y}$ + L' (K), $Na_3Ce_5Cl_{18}$ + $Ce_{1-y}Ba_yCl_{3-y}$ + $Ba_3Ce_2Cl_{12}$ (L), $Ce_{1-y}Ba_yCl_{3-y}$ + $Ba_3Ce_2Cl_{12}$ + L' (M). The dotted line corresponds to the binary system NaCl–$CeCl_3$.

Data availability

Data will be made available on request.

Acknowledgements

The authors of this paper gratefully acknowledge financial support from the ORANO group, as well as fruitful discussions with Dr. Elisa Capelli.

Appendix A. Mixing enthalpy estimation data

Experimental data on the mixing enthalpy of this system have not been reported in the literature. As mixing enthalpies are key data, however, to develop physically meaningful thermodynamic models, a method of estimating the mixing enthalpy was sought.

Several theories have been proposed to predict the mixing enthalpy of binary systems, such as those of Reiss, Katz and Kleppa [31], Blander [32] and Davis and Rice [27]. In a large experimental study by Østvold [33] the authors concluded that the overall most successful estimation method for the mixing enthalpy of binary fused salts was the method of Davis and Rice. Davis and Rice propose that the mixing enthalpy of a molten salt system is related to the size parameter δ_{12}, calculated with Eq. (A.1). In this equation, r^{cation_1} and r^{cation_2} are the sixfold-coordinated Shannon radii of the cations in a molten salt system, and r^{anion} is that of the anion.

$$\delta_{12} = \frac{r^{\text{cation}_1} - r^{\text{cation}_2}}{(r^{\text{cation}_1} + r^{\text{anion}})(r^{\text{cation}_2} + r^{\text{anion}})} \quad \text{(A.1)}$$

Davis suggested that the mixing enthalpy related linearly to δ_{12}. More recent work has shown that, while this is indeed true for simple binaries with relatively small cations, a second-order polynomial expression is often the more accurate choice [33–35] for larger ions. This work assumes that the relation between δ_{12} and the mixing enthalpy is indeed a second-order polynomial instead of a linear relation, as both Ba^{2+} and Ce^{3+} are relatively large cations. In order to obtain an estimate of the mixing enthalpy of the system $BaCl_2$–$CeCl_3$, data on similar systems i.e. $BaCl_2$–$RECl_3$ (RE = Rare Earth metals) or $AECl_2$–$CeCl_3$ (AE = Alkaline Earth metals) are necessary. These data are, however, also not available in the literature, and therefore have to be estimated first. The experimental data available in the literature have been reported by Enninga et al. [36] for the systems $AECl_2$–$RECl_3$ (AE = Mg, Ca; RE = La, Gd, Yb, Nd, Pr), and Blachnik et al. [37] for the systems $SrCl_2$–$RECl_3$ (RE = La, Gd, Yb).

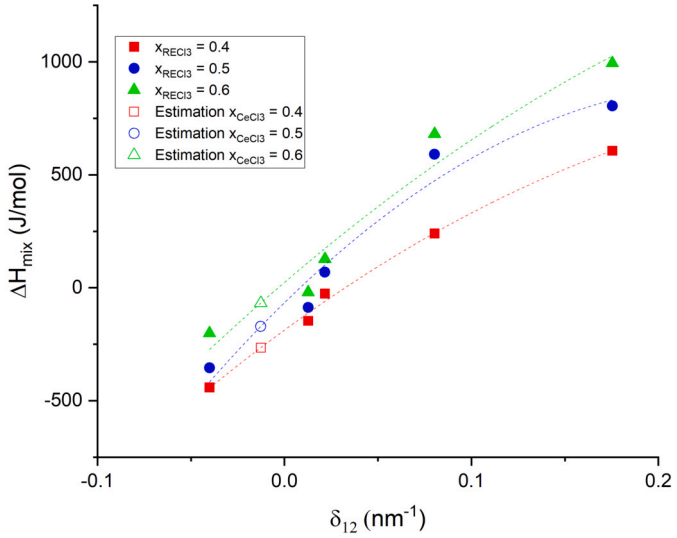

Fig. A.13. Mixing enthalpy of three compositions (x_{RECl3} = 0.4, 0.5 and 0.6) of the systems $CaCl_2$–$RECl_3$ (RE = La, Gd, Yb, Nd, Pr) [36,38] as a function of δ_{12} (filled symbols), as well as the interpolated value for the $CaCl_2$–$CeCl_3$ systems (empty symbols) at x_{RECl_3} = 0.4, 0.5, 0.6 respectively.

In the process of obtaining an estimate for the mixing enthalpy of $BaCl_2$-$CeCl_3$, estimates for the systems $AECl_2$–$CeCl_3$ (AE = Mg, Ca, Sr) were first made, as exemplified in Fig. A.13 for the Ca-systems. Using the estimated values, an extrapolation from the lighter alkaline earths (Mg, Ca, Sr) to barium can be performed, as shown in Fig. A.14 for the $AECl_2$–$LaCl_3$ (AE = Mg, Ca, Sr, Ba) systems. An example of an estimated mixing enthalpy curve using this method, along with experimental data reported in the literature, is given in Fig. A.15 for the $SrCl_2$–$RECl_3$ (RE = La, Gd, Yb, Ce) systems. Finally, the estimated curves for $AECl_2$–$CeCl_3$ (AE = Mg, Ca, Sr), as well as the desired estimation of the mixing enthalpy for $BaCl_2$–$CeCl_3$ are shown in Fig. A.16.

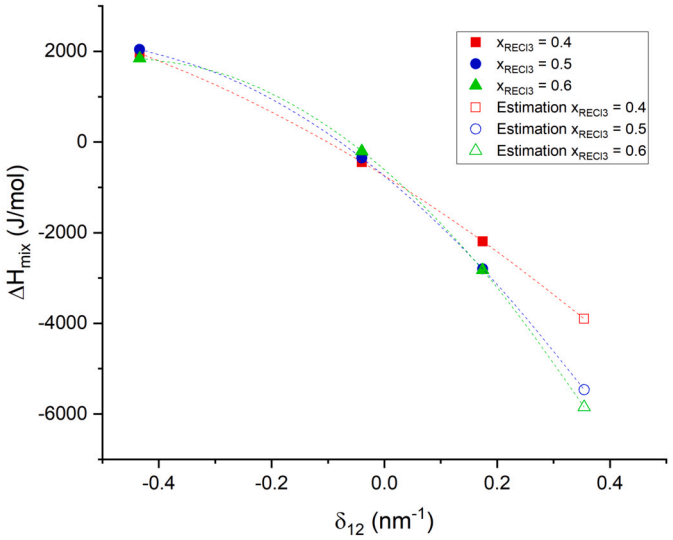

Fig. A.14. Mixing enthalpy of three compositions (x_{RECl3} = 0.4, 0.5 and 0.6) of the systems $AECl_2$–$LaCl_3$ (AE = Mg, Ca, Sr) [36,38] as a function of δ_{12} (filled symbols), as well as the extrapolated value for the $BaCl_2$–$LaCl_3$ system (empty symbols) at the same three compositions.

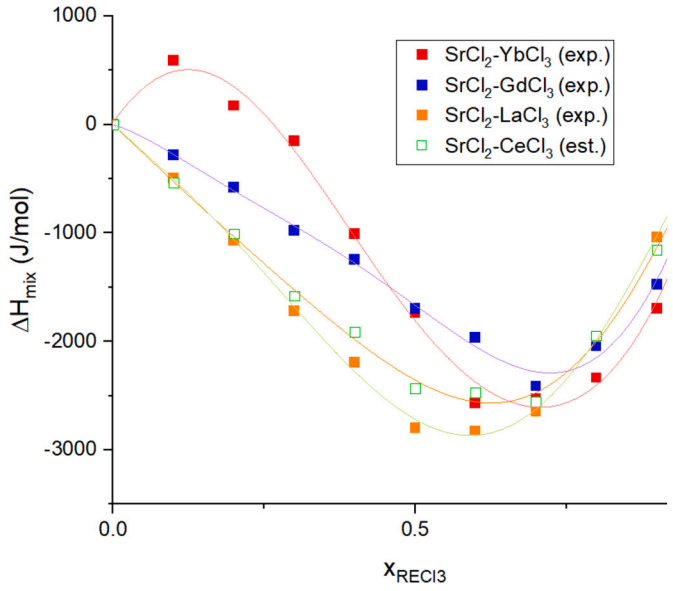

Fig. A.15. Interpolated data for the $SrCl_2$–$CeCl_3$ system using Davis' method (empty symbols), as well as the experimental data for $SrCl_2$–$RECl_3$ (RE = Yb, Gd, La) systems [36] used for this interpolation (filled symbols).

This extrapolation was performed for the composition range of 0-100% $CeCl_3$, calculating an estimate per step of 10% $CeCl_3$.

The data for the mixing enthalpy estimation of the systems investigated in this work come from various sources in the literature. Table A.12 shows the source where each set of data is reported, as well as the temperature at which the mixing enthalpy measurements were performed. All reported data were measured using some form of break-off ampoule experiments. The variation of the mixing enthalpy as a function of temperature is very small.

A.1. Phase equilibria in the presence of oxygen contamination

Since the intermediate that was found in this system reportedly contained oxygen according to Meyer et al. [25], it was deemed necessary

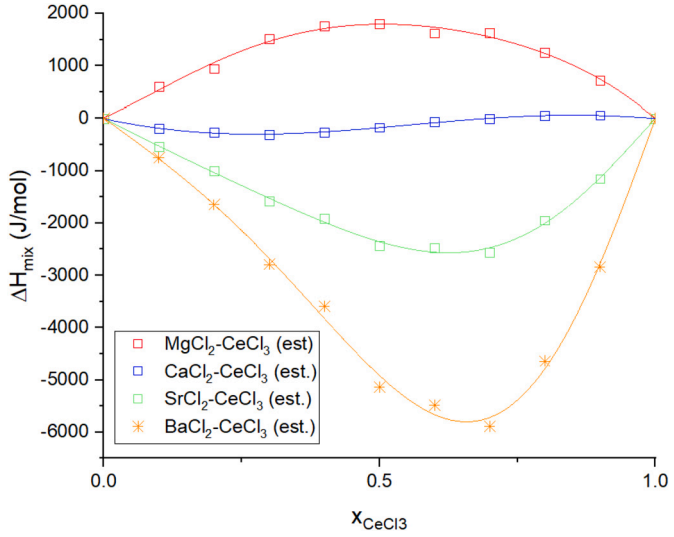

Fig. A.16. Extrapolated data for the $BaCl_2$–$CeCl_3$ system using Davis' method (asterisk symbols), as well as the estimated data of $AECl_2$–$CeCl_3$ (AE = Mg, Ca, Sr) systems used for this extrapolation (empty symbols).

Table A.12
Sources for mixing enthalpy data on the systems used in this work with the method by Davis and Rice [27].

Molten Salt System	Source	Temperature (K)
$CaCl_2$–$GdCl_3$	Enninga et al. [36]	1173
$CaCl_2$–$LaCl_3$	Enninga et al. [36]	1173
$CaCl_2$–$YbCl_3$	Enninga et al. [36]	1173
$CaCl_2$–$NdCl_3$	Gaune-Escard et al. [38]	1073
$CaCl_2$–$PrCl_3$	Gaune-Escard et al. [38]	1073
$MgCl_2$–$GdCl_3$	Enninga et al. [36]	1173
$MgCl_2$–$LaCl_3$	Enninga et al. [36]	1173
$MgCl_2$–$YbCl_3$	Enninga et al. [36]	1173
$SrCl_2$–$GdCl_3$	Blachnik et al. [37]	1180
$SrCl_2$–$LaCl_3$	Blachnik et al. [37]	1180
$SrCl_2$–$YbCl_3$	Blachnik et al. [37]	1180

to check the effect of possible oxygen contamination during the experiments performed herein. To this end, a DSC investigation of a mixture of $BaCl_2$ and $CeCl_3$ in a molar ratio of 3:1 was conducted in the presence of varying amounts oxygen, adding BaO acting as oxygen source.

The measured DSC curves of the samples containing BaO are shown in Fig. A.17. The DSC curves in Fig. A.17 show that the presence of BaO gives a significantly different response, and possibly inhibits the formation of the solid solution between $BaCl_2$ and $CeCl_3$. This is evidenced by the disappearance of the peak at T = 950 K upon addition of BaO. Furthermore, the peritectic event that was measured in the oxygen-free sample and the sample with 2% BaO disappears upon further addition of BaO. This indicates that an excess of BaO could inhibit the formation of the intermediate.

The measured sample containing 10% BaO was subjected to an XRD analysis to investigate which phases had formed during the experiment, and a profile refinement was performed. This refinement is shown in Fig. A.18, and the phases that are present are $BaCl_2$, $Ba_3Ce_2Cl_{12}$ and CeOCl. The presence of CeOCl suggests that a possible oxygen contamination would manifest itself in the form of this oxychloride. This compound, however, has not been observed in any of the XRD analyses of this system without the addition of BaO.

In conclusion, based on the change in DSC response as seen in Fig. A.17, as well as the apparent formation of CeOCl as shown in Fig. A.18, it is unlikely that the samples measured in this work were contaminated with oxygen.

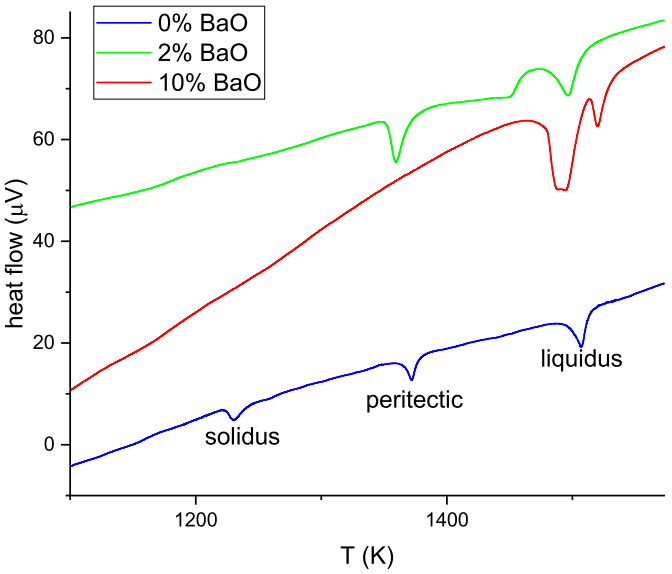

Fig. A.17. Calorimetry curves measured using DSC of three samples containing a mixture of $BaCl_2$ and $CeCl_3$ in a set stoichiometric ratio of 3:1, with varying amount of BaO contamination: 0_{mol}% BaO (blue, bottom), 1.5_{mol}% BaO (green, top) and 10_{mol}% BaO (red, middle).

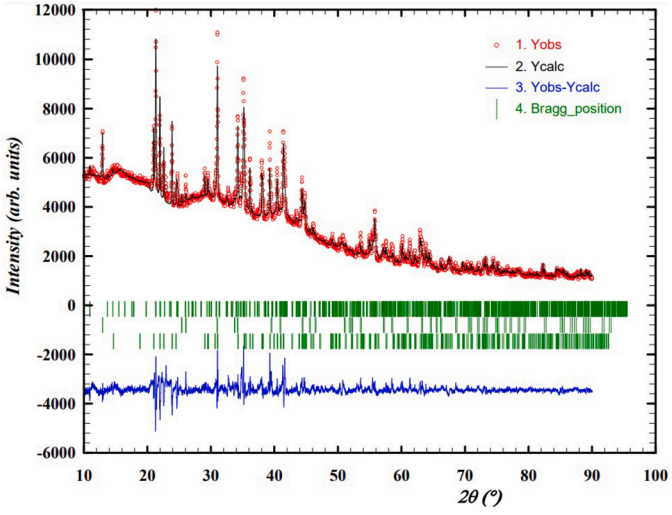

Fig. A.18. Profile refinement of the sample with 10% BaO. The observed intensity (Yobs, red) is plotted along with the calculated intensity from the refinement (Ycalc, black), and the difference between the two is shown (Yobs-Ycalc, blue). The angles at which reflections occur are shown as well (Bragg positions, vertical lines). Measurement at λ = Cu-Kα. Present phases are $BaCl_2$, $Ba_3Ce_2Cl_{12}$ and CeOCl.

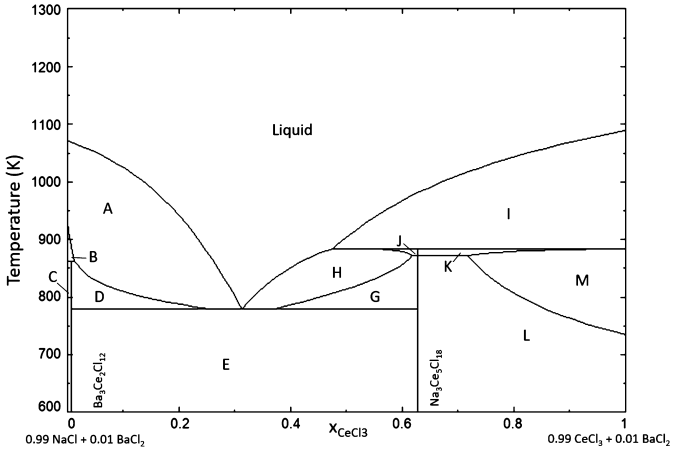

Fig. B.19. Phase diagram of the {0.99 NaCl + 0.01 $BaCl_2$}-{0.99 $CeCl_3$ + 0.01 $BaCl_2$} pseudo-binary section of the NaCl–$BaCl_2$–$CeCl_3$ ternary system. The labelled phases are NaCl + L' (A), NaCl + $BaCl_2$ + L' (B), $BaCl_2$ + $Ba_3Ce_2Cl_{12}$ + NaCl (C), NaCl + $Ba_3Ce_2Cl_{12}$ + L' (D), NaCl + $Na_3Ce_5Cl_{18}$ + $Ba_3Ce_2Cl_{12}$ (E), $Na_3Ce_5Cl_{18}$ + $Ba_3Ce_2Cl_{12}$ + L' (G), $Na_3Ce_5Cl_{18}$ + L' (H), $Ce_{1-y}Ba_yCl_{3-y}$ + L' (I), $Na_3Ce_5Cl_{18}$ + $Ba_{1-x}Ce_xCl_{2+x}$ + L' (J), $Na_3Ce_5Cl_{18}$ + $Ce_{1-y}Ba_yCl_{3-y}$ + L' (K), $Na_3Ce_5Cl_{18}$ + $Ce_{1-y}Ba_yCl_{3-y}$ + $Ba_3Ce_2Cl_{12}$ (L), $Ce_{1-y}Ba_yCl_{3-y}$ + $Ba_3Ce_2Cl_{12}$ + L' (M).

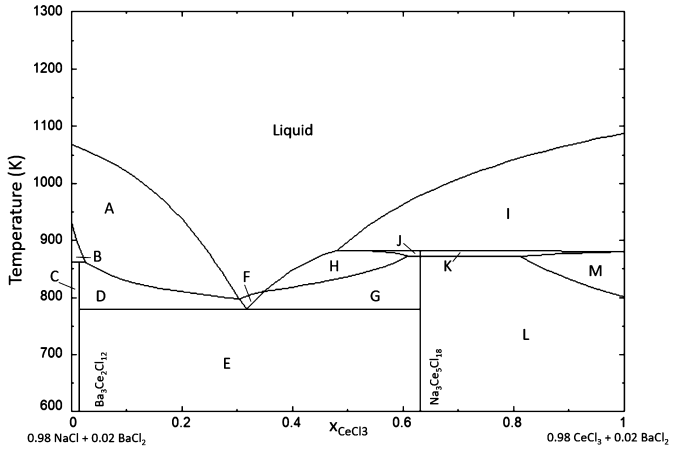

Fig. B.20. Phase diagram of the {0.98 NaCl + 0.02 $BaCl_2$}-{0.98 $CeCl_3$ + 0.02 $BaCl_2$} pseudo-binary section of the NaCl–$BaCl_2$–$CeCl_3$ ternary system. The labelled phases are NaCl + L' (A), NaCl + $BaCl_2$ + L' (B), $BaCl_2$ + $Ba_3Ce_2Cl_{12}$ + NaCl (C), NaCl + $Ba_3Ce_2Cl_{12}$ + L' (D), NaCl + $Na_3Ce_5Cl_{18}$ + $Ba_3Ce_2Cl_{12}$ (E), $Ba_3Ce_2Cl_{12}$ + L' (F), $Na_3Ce_5Cl_{18}$ + $Ba_3Ce_2Cl_{12}$ + L' (G), $Na_3Ce_5Cl_{18}$ + L' (H), $Ce_{1-y}Ba_yCl_{3-y}$ + L' (I), $Na_3Ce_5Cl_{18}$ + $Ba_{1-x}Ce_xCl_{2+x}$ + L' (J), $Na_3Ce_5Cl_{18}$ + $Ce_{1-y}Ba_yCl_{3-y}$ + L' (K), $Na_3Ce_5Cl_{18}$ + $Ce_{1-y}Ba_yCl_{3-y}$ + $Ba_3Ce_2Cl_{12}$ (L), $Ce_{1-y}Ba_yCl_{3-y}$ + $Ba_3Ce_2Cl_{12}$ + L' (M).

Appendix B. Ternary field investigations

In section 5.7, the pseudo-binary system {0.95 NaCl + 0.05 $BaCl_2$}-{0.95 $CeCl_3$ + 0.05 $BaCl_2$} has been presented, which is equivalent to the binary NaCl–$CeCl_3$ upon addition of 5% $BaCl_2$. The pseudo-binary phase diagrams of NaCl–$CeCl_3$ upon addition of 1%, 2%, 3% and 4% $BaCl_2$ are presented here in Figs. B.19-B.22. Fig. B.23 shows the projected liquidus surface of the ternary NaCl–$BaCl_2$–$CeCl_3$.

Fig. B.19 shows that the addition of 1% of $BaCl_2$ has very little adverse effects on the melting behaviour of the binary NaCl–$CeCl_3$, with the eutectic being approximately the same as in the pure system. Upon further addition of $BaCl_2$, Figs. B.20-B.22, the eutectic temperature increases, and precipitation of the fissile species becomes more likely. The liquidus projection in Fig. B.23 shows that the addition of very small amounts of $BaCl_2$ ($\lesssim$ 1%) does indeed not influence the melting point of the eutectic in a significant way. Further addition of $BaCl_2$, however, does quickly lead to an increase of the eutectic temperature, and allows for the formation of the intermediate $Ba_3Ce_2Cl_{12}$.

Appendix C. Supplementary material

Supplementary material related to this article can be found online at https://doi.org/10.1016/j.molliq.2024.123997.

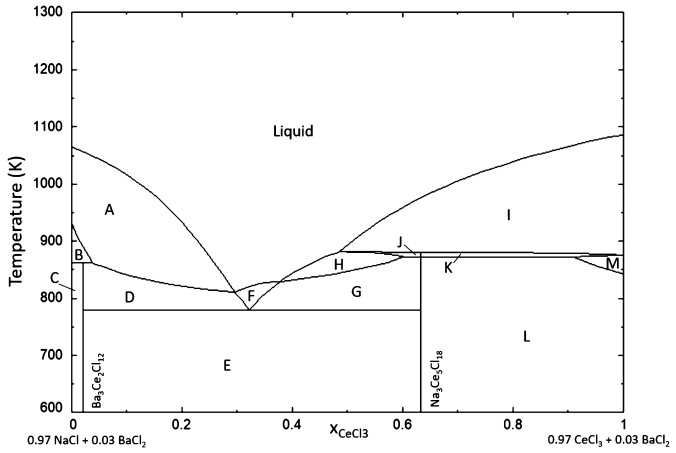

Fig. B.21. Phase diagram of the {0.97 NaCl + 0.03 $BaCl_2$}-{0.97 $CeCl_3$ + 0.03 $BaCl_2$} pseudo-binary section of the NaCl–$BaCl_2$–$CeCl_3$ ternary system. The labelled phases are NaCl + L' (A), NaCl + $BaCl_2$ + L' (B), $BaCl_2$ + $Ba_3Ce_2Cl_{12}$ + NaCl (C), NaCl + $Ba_3Ce_2Cl_{12}$ + L' (D), NaCl + $Na_3Ce_5Cl_{18}$ + $Ba_3Ce_2Cl_{12}$ (E), $Ba_3Ce_2Cl_{12}$ + L' (F), $Na_3Ce_5Cl_{18}$ + $Ba_3Ce_2Cl_{12}$ + L' (G), $Na_3Ce_5Cl_{18}$ + L' (H), $Ce_{1-y}Ba_yCl_{3-y}$ + L' (I), $Na_3Ce_5Cl_{18}$ + $Ba_{1-x}Ce_xCl_{2+x}$ + L' (J), $Na_3Ce_5Cl_{18}$ + $Ce_{1-y}Ba_yCl_{3-y}$ + L' (K), $Na_3Ce_5Cl_{18}$ + $Ce_{1-y}Ba_yCl_{3-y}$ + $Ba_3Ce_2Cl_{12}$ (L), $Ce_{1-y}Ba_yCl_{3-y}$ + $Ba_3Ce_2Cl_{12}$ + L' (M).

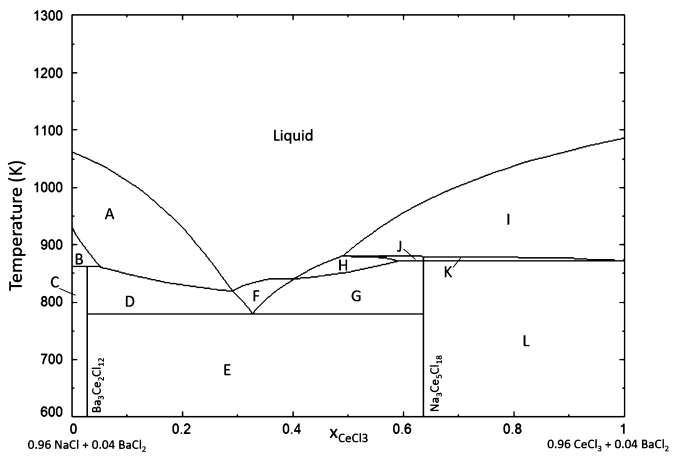

Fig. B.22. Phase diagram of the {0.96 NaCl + 0.04 $BaCl_2$}-{0.96 $CeCl_3$ + 0.04 $BaCl_2$} pseudo-binary section of the NaCl–$BaCl_2$–$CeCl_3$ ternary system. The labelled phases are NaCl + L' (A), NaCl + $BaCl_2$ + L' (B), $BaCl_2$ + $Ba_3Ce_2Cl_{12}$ + NaCl (C), NaCl + $Ba_3Ce_2Cl_{12}$ + L' (D), NaCl + $Na_3Ce_5Cl_{18}$ + $Ba_3Ce_2Cl_{12}$ (E), $Ba_3Ce_2Cl_{12}$ + L' (F), $Na_3Ce_5Cl_{18}$ + $Ba_3Ce_2Cl_{12}$ + L' (G), $Na_3Ce_5Cl_{18}$ + L' (H), $Ce_{1-y}Ba_yCl_{3-y}$ + L' (I), $Na_3Ce_5Cl_{18}$ + $Ba_{1-x}Ce_xCl_{2+x}$ + L' (J), $Na_3Ce_5Cl_{18}$ + $Ce_{1-y}Ba_yCl_{3-y}$ + L' (K), $Na_3Ce_5Cl_{18}$ + $Ce_{1-y}Ba_yCl_{3-y}$ + $Ba_3Ce_2Cl_{12}$ (L).

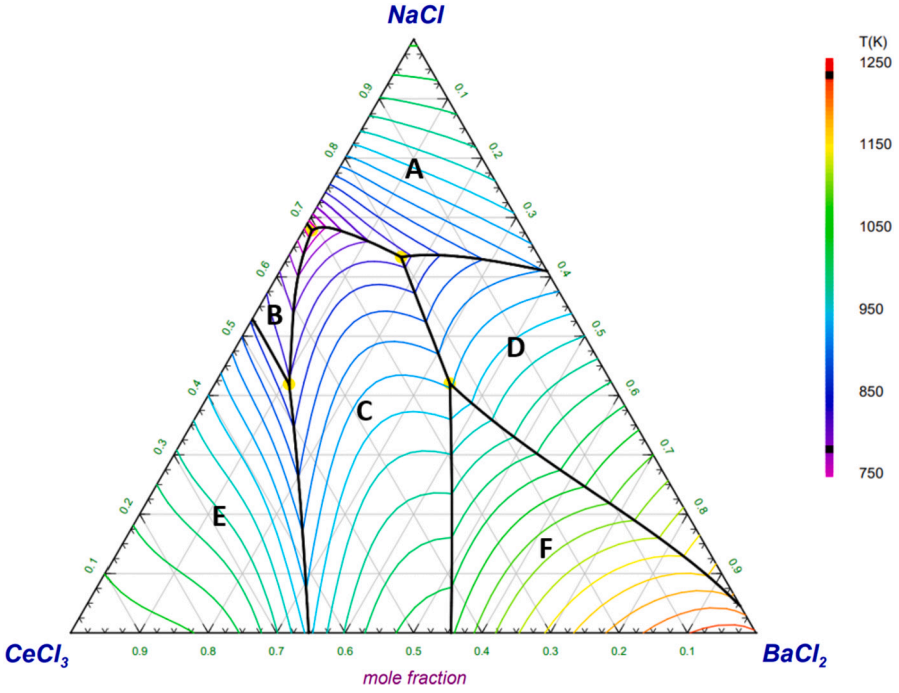

Fig. B.23. Projected liquidus surface of the NaCl–$BaCl_2$–$CeCl_3$ ternary system. Precipitate target phases labelled A-F are: NaCl (A), $Na_3Ce_5Cl_{18}$ (B), $Ba_3Ce_2Cl_{12}$ (C), $BaCl_2$ (D), $Ce_{1-y}Ba_yCl_{3-y}$ (E), $Ba_{1-x}Ce_xCl_{2+x}$ (F).

References

[1] E. Bettis, R. Schroeder, G. Cristy, H. Savage, R. Affel, L. Hemphill, The aircraft reactor experiment—design and construction, Nucl. Sci. Eng. 2 (6) (1957) 804–825.

[2] C. Le Brun, Molten salts and nuclear energy production, J. Nucl. Mater. 360 (1) (2007) 1–5.

[3] J.W. Mcmurray, K. Johnson, C. Agca, B.R. Betzler, D.J. Kropaczek, T.M. Besmann, D. Andersson, N. Ezell, Roadmap for thermal property measurements of Molten salt reactor systems, Tech. Rep., Oak Ridge National Lab. (ORNL), Oak Ridge, TN (United States), 2021.

[4] D. Holcomb, G. Flanagan, B. Patton, J. Gehin, R. Howard, T. Harrison, Fast spectrum Molten salt reactor options, ORNL/TM-2011/105, 2011.

[5] M. Taube, Fast reactors using Molten chloride salts as fuel, Tech. Rep., INFCE, Switzerland, 1978.

[6] E. Sooby, A. Nelson, J. White, P. McIntyre, Measurements of the liquidus surface and solidus transitions of the nacl–ucl3 and nacl–ucl3–cecl3 phase diagrams, J. Nucl. Mater. 466 (2015) 280–285.

[7] M.W. Chase Jr, Nist-janaf thermochemical tables, J. Phys. Chem. Ref. Data, Monogr. 9 (1998).

[8] R. Konings, A. Kovács, Thermodynamic properties of the lanthanide (iii) halides, Handb. Phys. Chem. Rare Earths 33 (2003) 147–247.

[9] H.M. Rietveld, A profile refinement method for nuclear and magnetic structures, J. Appl. Crystallogr. 2 (2) (1969) 65–71.

[10] B. van Laar, H. Schenk, The development of powder profile refinement at the reactor centre Netherlands at Petten, Acta Crystallogr., Sect. A, Found. Adv. 74 (2) (2018) 88–92.

[11] J. Rodríguez-Carvajal, Recent advances in magnetic structure determination by neutron powder diffraction, Physica B, Condens. Matter 192 (1–2) (1993) 55–69.

[12] L. Van Eijck, L. Cussen, G. Sykora, E. Schooneveld, N. Rhodes, A. Van Well, C. Pappas, Design and performance of a novel neutron powder diffractometer: Pearl at tu Delft, J. Appl. Crystallogr. 49 (5) (2016) 1398–1401.
[13] G. Höhne, H. Cammenga, W. Eysel, E. Gmelin, W. Hemminger, The temperature calibration of scanning calorimeters, Thermochim. Acta 160 (1) (1990) 1–12.
[14] G. Della Gatta, M.J. Richardson, S.M. Sarge, S. Stølen, Standards, calibration, and guidelines in microcalorimetry. Part 2. Calibration standards for differential scanning calorimetry* (iupac technical report), Pure Appl. Chem. 78 (7) (2006) 1455–1476.
[15] M.I. Kilday, The Enthalpy of Solution of SRM 1655 (KCl) in H2O, J. Res. Natl. Inst. Stand. Technol. 85 (6) (1980) 467–482.
[16] I. Wadsö, R.N. Goldberg, Standards in isothermal microcalorimetry (iupac technical report), Pure Appl. Chem. 73 (10) (2001) 1625–1639.
[17] D.D. Wagman, W.H. Evans, V.B. Parker, R.H. Schumm, I. Halow, S.M. Bailey, K.L. Churney, R.L. Nuttall, The nbs tables of chemical thermodynamic properties selected values for inorganic and c1 and c2 organic substances in si units, J. Phys. Chem. Ref. Data 11 (2) (1982).
[18] H.L. Lukas, S.G. Fries, B. Sundman, et al., Computational Thermodynamics: the Calphad Method, vol. 131, Cambridge University Press, 2007.
[19] Centre for Research in Computational Thermochemistry, Factsage 7.2 [Online]. Available: http://www.factsage.com.
[20] V. Glushko, L. Gurvich, V. Weitz, et al., Thermodynamic Properties of Individual Substances, vol. 3, no. 2, Nauka Publishing House, Moscow, 1978.
[21] I. Morozov, F.N. T'en, Types of equilibrium diagram of binary systems of r.e.e. and alkaline-Earth metal chlorides, Russ. J. Inorg. Chem. 16 (8) (1971) 1215–1217.
[22] I. Storonkin, O. Vasilkova, I. Kozhina, Thermal and X-ray studies of the barium chloride sodium chloride—cerium (iii) chloride system, Vestn. Leningr. Univ. 4 (1973) 80–83.
[23] A.D. Pelton, P. Chartrand, G. Eriksson, The modified quasi-chemical model: part iv. Two-sublattice quadruplet approximation, Metall. Mater. Trans. A 32 (6) (2001) 1409–1416.
[24] O. Beneš, Thermodynamic database on Molten salt reactor systems, technical report, European Commission, Joint Research Centre, 2021.
[25] G. Meyer, S. Masselmann, The alkali-poor part of the pseudoternary triangle $AX/BX_2/MX_3$: crystal structures, properties, and potentials of (alkali)/alkaline-Earth/rare-Earth chloride materials, Chem. Mater. 10 (10) (1998) 2994–3004.
[26] J. Zhang, Y. Sun, M. Guan, Z. Qiao, Thermodynamic optimization of the $CeCl_3$–$AECl_2$ (AE=Mg,Ca,Sr,Ba) phase diagrams, Calphad 27 (3) (2003) 305–308.
[27] H.T. Davis, S.A. Rice, Perturbation theory of the heats of mixing of fused salts, J. Chem. Phys. 41 (1) (1964) 14–24.
[28] R.D. Shannon, Revised effective ionic radii and systematic studies of interatomic distances in halides and chalcogenides, Acta Crystallogr., Sect. A Cryst. Phys. Diffr. Theor. Gen. Crystallogr. 32 (5) (1976) 751–767.
[29] P. Chartrand, A.D. Pelton, Thermodynamic evaluation and optimization of the licl-nacl-kcl-rbcl-cscl-mgcl2-cacl2-srcl2-bacl2 system using the modified quasichemical model, Can. Metall. Q. 40 (1) (2001) 13–32.
[30] G. Lu, C. Robelin, P. Chartrand, M. He, K. Wang, Thermodynamic evaluation and optimization of the (licl+ nacl+ kcl+ mgcl2+ cacl2+ cecl3) system, Fluid Phase Equilib. 487 (2019) 83–97.
[31] H. Reiss, J. Katz, O. Kleppa, Theory of the heats of mixing of certain fused salts, J. Chem. Phys. 36 (1) (1962) 144–148.
[32] M. Blander, Excess free energies and heats of mixing in certain Molten salt mixtures, J. Chem. Phys. 37 (1) (1962) 172–173.
[33] T. Østvold, A Thermodynamic Study of Some Fused Salt Mixtures Containing Alkali and Alkaline Earth Chlorides, Bromides and Iodides, vol. 91, Institute of Physical Chemistry, University of Trondheim, NTH, 1971.
[34] G. Papatheodorou, O. Kleppa, Thermodynamic studies of binary charge unsymmetrical fused salt systems. Cerium (iii) chloride-alkali chloride mixtures, J. Phys. Chem. 78 (2) (1974) 178–181.
[35] J. Schorne-Pinto, J.A. Yingling, M.S. Christian, A.M. Mofrad, M.A. Aslani, T.M. Besmann, Correlational approach to predict the enthalpy of mixing for chloride melt systems, ACS Omega (2021).
[36] E. Enninga, G. Alberts, R. Blachnik, Thermochemistry of mixtures of lanthanoid chlorides with chlorides of some divalent cations, Thermochim. Acta 64 (3) (1983) 317–325.
[37] R. Blachnik, G. Alberts, E. Enninga, Zur kenntnis der zustandsdiagramme $SECl_3/MCl_2$, (SE=La,Sm,Gd,Yb;M=Sr,Ba), Z. Anorg. Allg. Chem. 522 (3) (1985) 207–216.
[38] M. Gaune-Escard, L. Rycerz, M. Hoch, Analysis of the enthalpy of mixing data of binary and ternary rare Earth (dy, nd, pr, tb)—alkali metal halide systems, J. Mol. Liq. 83 (1–3) (1999) 83–94.